Role of Physical and Chemical Interactions in the Behavior of Supported Metal Catalysts: Iron on Alumina—A Case Study

I. SUSHUMNA AND E. RUCKENSTEIN[1]

Department of Chemical Engineering, State University of New York, Buffalo, New York 14260

Iron, being the most reactive of the group VIII metals, has been chosen to examine the role of strong chemical interactions between gas, crystallite, and substrate in the behavior of supported metal crystallites. Model catalysts of iron deposited by vacuum evaporation onto thin films of alumina have been heated in ultrahigh pure hydrogen (which, however, contains traces of O_2 and moisture), in additionally purified hydrogen (to eliminate or minimize the above impurities), in oxygen, and alternately in H_2 and O_2. Transmission electron micrographs provide information on the behavior and shape of the crystallites and electron diffraction provides information on the chemical compounds formed. It is shown that iron oxide which forms even in hydrogen containing traces of oxygen and/or moisture undergoes strong chemical interaction with alumina to form solid solutions or/and stoichiometric aluminates. Such chemical interactions lead to enhanced surface spreading phenomena and to unusual shapes of the crystallites. The role of strong chemical interactions in the wetting behavior of the crystallites is examined in some detail. It is suggested that because of these interactions the interfacial tension between crystallite and substrate can be decreased enormously (it may even become negative under nonequilibrium conditions). This then leads to a rapid spreading of the crystallite over the substrate, to torus formation, and/or fragmentation of the crystallite. At high temperatures, the smaller crystallites spread completely over the substrate and, as inferred from the electron micrographs, a multilayer film appears to coexist with the crystallites. A variety of mechanisms of sintering could be identified, such as migration and coalescence (even crystallites over 400 Å in size were observed to migrate occasionally), direct ripening, and Ostwald ripening. However, the micrographs indicate that these processes, as well as redispersion, are not simple, but parts of complex surface phenomena involving chemical interactions, wetting, shape changes, splitting etc. © 1985 Academic Press, Inc.

INTRODUCTION

Currently, metal catalysts are being prepared mostly in a highly dispersed, supported form replacing the old fused or unsupported powder types. While the commonly used refractory oxide supports, silica and alumina, increase the metal dispersion, they are not inert especially toward the non-noble metals (*1*). The chemical reactivity between the active metal and the oxide support in turn affects the particle size distribution and consequently the activity and selectivity of the catalyst. Iron, the most electropositive of the group VIII elements and consequently a very reactive

metal, is employed extensively as a catalyst in such important industrial processes as ammonia synthesis, the recently rejuvenated Fischer–Tropsch synthesis, and other hydrogenation and dehydrogenation reactions (*2*). Traditionally, iron is deposited onto the oxide supports in the form of ferric salts, prior to calcination and reduction at high temperatures (*3, 12*). When present as Fe^{3+} ions, iron exhibits strong reactivity with the support, especially with alumina because of the chemical similarity between Fe^{3+} and Al^{3+} ions (*4, 5*). Consequently, at low loadings on alumina, iron is not reduced easily to the zero-valent state, because a large fraction of the iron ions interact strongly with the substrate. The strength of the interactions between the ac-

[1] To whom correspondence should be addressed.

tive-metal ion and the support and consequently the reducibility and the particle size of the supported iron catalyst depend upon the chemical precursor used, the catalyst pretreatment (particularly the temperature of decomposition), and the metal loading. For example, Garten and Ollis (6) have shown, for samples prepared by impregnation, that when the metal loading on alumina is low (0.05%), the ferric ions can be reduced only to the ferrous state, even when the reduction with hydrogen occurs at temperatures as high as 700°C. On the other hand, Brenner and Hucul (7) have observed that the decomposition at low temperatures (<150°C) of zero-valent iron complexes, such as the iron carbonyls, adsorbed on alumina, yields highly dispersed iron catalysts. In this case the initial dispersion can be more than an order of magnitude higher than that of the catalyst prepared by the more traditional method of impregnation with ferric ions, but, because of the weaker interactions with the support, the zero valent particles may sinter more easily. Raupp and Delgass (8) have shown that mild pretreatment of the impregnated catalysts by slow vacuum drying, prior to reduction, produces significantly smaller particles of iron in the case of Fe/SiO_2. The nonreducibility and/or the smaller particle sizes arising as a result of the interactions between metal and support can have important consequences on the activity and selectivity of the supported iron catalysts in the Fischer–Tropsch reaction (8–11).

The literature abounds in Mössbauer spectroscopic investigations of supported iron catalysts, especially regarding their role in the Fischer–Tropsch reaction (11–14). Mössbauer spectroscopy is a powerful tool to characterize catalysts involving ferromagnetic metals. Nonetheless, when a strong interaction between metal and support exists, the interpretation of the spectra becomes difficult regarding both the particle size distribution and the exact chemical compounds formed (15). In addition, information regarding the microstructure and

the shape of the particles cannot be obtained (16). A complementary technique such as electron microscopy can provide both the size distribution and the shape of the particles and, via electron diffraction, can also identify the chemical compounds formed. Electron microscopy and electron diffraction have been used in the present paper to investigate the behavior of a model Fe/Al_2O_3 catalyst and results are presented regarding the physicochemical changes accompanying their heating at different temperatures in a reducing (H_2) atmosphere, in an oxidizing (O_2) atmosphere, and during an alternate heating in these atmospheres. The present investigation emphasizes the role of the surface phenomena and of the chemical interactions in the complex processes observed with model Fe/Al_2O_3 catalysts. Accordingly, the electron micrographs, which provide physical information on shape and size, are supplemented with chemical infomation on the compounds formed via electron diffraction.

EXPERIMENTAL

Preparation of model alumina supports. Electron-transparent and nonporous films of amorphous Al_2O_3 were prepared by anodically building up the oxide on a clean, thin, high-purity aluminum foil (99.999%, Alfa Products Inc.) and stripping the oxide film off by dissolving the unoxidized aluminum in a dilute mercuric chloride solution (21). The oxide films were washed in distilled water and picked up on gold electron-microscope grids. They were subsequently heated in air at 800°C for 72 h to transform the amorphous alumina into the γ or η form and also to ensure that no further changes would occur during its subsequent use.

Deposition of the active metal. Iron films of different thicknesses were deposited onto the alumina substrates by evaporating the corresponding amounts of 99.998% pure iron wire (Alfa Products Inc.) from a tungsten basket in an Edwards vacuum evaporator under a vacuum of better than 2 × 10^{-6} Torr. The thickness of the metal film

deposited was estimated from the amount of metal evaporated and the distance between the source and the target. The substrate was kept at room temperature during deposition.

Heat treatment. Samples were heated in a quartz boat inside a 3.8-cm-diameter and 120-cm-long quartz tube. A predetermined gas flowed through the quartz tube during heating and its flow rate of 150 cm^3/min was maintained constant during the heat treatment. The gases used in the experiments were all ultrahigh purity (UHP) grade, supplied by Linde Division, Union Carbide Corporation. Hydrogen, 99.999% pure, contained less than 1 ppm O$_2$ and less than 2 ppm moisture. Helium, also 99.999% pure, contained less than 3 ppm moisture. For some experiments, the hydrogen was further purified by passing it through a Deoxo unit (Englehard Industries) followed by a silica gel column and then through a 5A molecular sieve bed immersed in liquid nitrogen. Helium was also purified by passing it through the liquid-nitrogen trap.

After introducing the boat containing the sample into the reactor, each heat treatment followed the sequence: flushing the reactor with helium for at least 5 min; heating the specimen from room temperature to the desired value in a helium atmosphere, switching over the gas stream to hydrogen or oxygen as desired and heating for the predetermined length of time, and cooling down the specimen slowly to room temperature in a helium atmosphere before it is withdrawn for observation. Following each heat treatment, the same regions of the sample were photographed using a JEOL 100U transmission electron microscope. During each observation, the entire specimen area was scanned to check if the behavior was uniform throughout. Electron diffraction patterns were obtained for all the specimens after each treatment.

RESULTS AND DISCUSSION

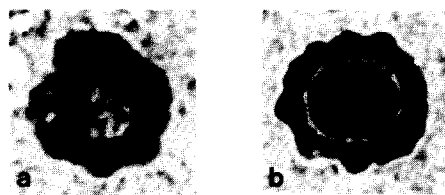Several samples have been investigated at each of the following loadings corre-

FIG. 1. Representation of (a) torus and (b) core-and-ring structures.

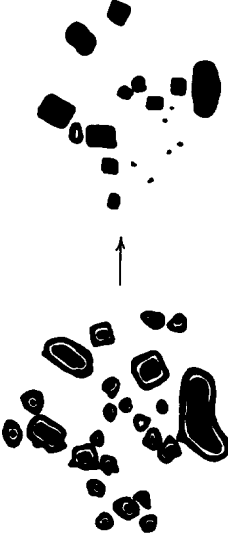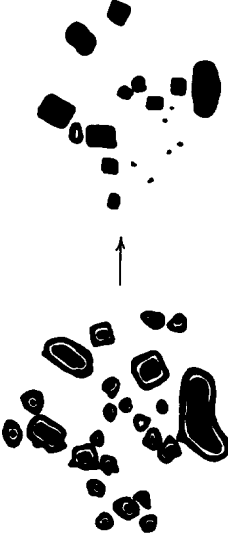sponding to film thicknesses of 5, 6, 7.5, 10, and 12.5 Å. Except for the cases in which the behavior was different, the results are reported for either 6- or 7.5-Å loadings. A large number of events have been observed at each of the temperatures investigated regarding the sintering and the wetting behavior as well as the changes in the shape of crystallites following heating in hydrogen, oxygen, and alternate heating in these two atmospheres. Table 1 summarizes the various events observed. Tables 2 to 5 provide the events observed under various conditions, the chemical compounds identified, and the corresponding micrograph numbers. The torus and core-and-ring structures, to which we refer frequently later in the text, are represented in Figs. 1a and b.

A. Behavior with as-Supplied Hydrogen

A.1. Heating in Hydrogen. It is seen from Table 2 that distinct crystallites do not form easily at 300°C, whereas at 400°C they form after heating for only 1 h. At both temperatures, a compound whose d values lie between those of γ-Fe$_2$O$_3$ (Fe$_3$O$_4$) and the higher aluminate, Al$_2$Fe$_2$O$_6$, is detected, in addition to other compounds. (γ-Fe$_2$O$_3$ and Fe$_3$O$_4$ have the same lattice constant and therefore cannot be easily differentiated by electron diffraction). It is to be noted that the major d values of Al$_2$Fe$_2$O$_6$ are greater than those of γ-Fe$_2$O$_3$ (Fe$_3$O$_4$). Therefore, an increase in the major d values from those of γ-Fe$_2$O$_3$ toward those of Al$_2$Fe$_2$O$_6$ would indicate the formation of solid solutions of iron oxide in alumina ultimately leading to

TABLE 1

Types of Events Observed

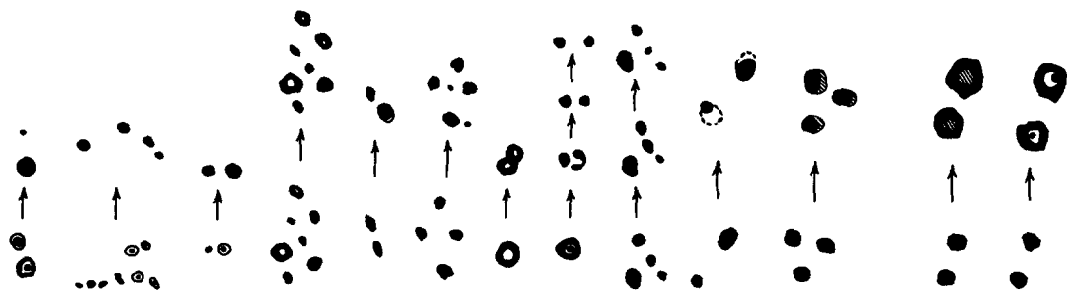| Type	Event and figure number	Schematic of the events	
		Before	After
A	Coalescence of nearby particles. Appearance of dumbbell-shape particles (2f–2i; 3a–c; 4a, 4b; 8a–c; 13b–d)		
B	Migration with subsequent coalescence (3a–c; 7b, c; 13a–d) (or, coalescence followed by migration)		
C	Migration without coalescence (4'c, d; 6d, e; 7b, c; 11a, b; 13b, c)		
D.a	Decrease and disappearance of a few smaller particles (Localized ripening between a few particles. Direct ripening) (3a, b; 4'a–c)		
D.b	Ripening between particles of almost the same size. Probably due to local curvature difference (3a, b; 4'a–c)		
D.c	Transfer of molecules via a narrow, whisker-like bridge or a neck formed between two particles (3a, b; 4'a–c)		
E	Decrease and disappearance of a large number of small particles. (Global ripening, Ostwald ripening; break-up to unresolved crystallites and their migration; extension to undetectable islands.) (4a–d; 12a–c)		
F	Considerable sintering with redistribution of particles over some areas of the specimen (7b, c)		

G Decrease in size or disappearance of a particle with no obvious growth of nearby particles (3a, b; 4a, b; 6d, e)

H Disappearance of large particles without decreasing in size first; A large particle nearby a smaller particle decreases in size and/or disappears or coalesces with the latter. The smaller particle either increases in size or remains unaffected (3a–c; 13a–d)

I Disappearance of small as well as large particles (3a, b; 4a, b; 13a, b)

J Growth of some small particles (3b, c)

K Increase in contrast (darkening) of all particles. (Growth of all particles small and large); Light and thin particles grow bigger and darker. (6b, c; 7a, b)

L Appearance of new particles. (6e, f; 12a–d; 13a–c)

M Splitting of particles without complete separation of the units. (2g–i; 13b–d)

N Splitting of particles with separation and migration. (6d–f; 13a, b)

O Extension of small particles; recontraction of the extended particles. (2b–e; 13c, d)

P Appearance of periphery marks around particles. (7c; 9b, c)

Q Appearance of a film extending out from around the particles. (12a, b)

R Substrate grain boundaries appear less distinct on heating in oxygen. A film appears to cover the substrate. The grain boundaries appear sharp again on heating in hydrogen subsequently. (12a, c, d; 15c, d, e)

S.a Considerable extension of the crystallite to result in a torus shape. (4e; 9a; 10b)

S.b Considerable extension and appearance of a torus shape with a small remnant particle in the cavity. (14b, d; 15a)

TABLE 1—*Continued*

Type	Event and figure number	Schematic of the events	
		Before	After
T	Considerable extension to a kind of thick film with a remnant particle on top. (14b, d; 15d, e)		
U	Rupture of crystallites. The crystallite is composed of very small particles held close-together making it appear porous. (8c, d; 9d–f; 15d, e)		
V	Break-up of the crystallites with the subunits interconnected. The sub-units coalesce subsequently. (9a, b; 10b–d; 15a, b)		
W	Considerable break-up of the crystallites to very small pieces. (9g)		
X	Contraction of periphery marks to form small particles. (11c)		
Y	Faceting of particles. (11c)		

TABLE 2

Heating in As-Supplied Hydrogen

Total heating time	Event observed	Compound identified
Table 2$_{6,300}$^{a}		
1 h	No distinct large particle formation	γ-Al$_2$O$_3$
Up to 9 h	No detectable change after heating in a few steps, except for changes in chemical composition.	FeO · Al$_2$O$_3$ (FeAl$_2$O$_4$) and solid solution of Fe$_2$O$_3$ in Al$_2$O$_3$ approaching Al$_2$Fe$_2$O$_6$
Table 2$_{6,400}$		
$\frac{1}{2}$ h	Scattered, light, small, and large particles with torus shape observed. (2a)^b	FeO · Al$_2$O$_3$ and traces of Fe$_3$O$_4$ (γ-Fe$_2$O$_3$)
1 h	An increase in number of large and distinct crystallites. Some particles acquire the core-and-ring structure. (2b)	
2 h	Increase in size and darkening of small and large crystallites. Particles have a torus shape and are of uniform size. No change in the number of particles. (2c)	An increase in the intensity of FeAl$_2$O$_4$ rings and a decrease in the intensity of Fe$_3$O$_4$ rings
Up to 36 h	Considerable extension of some particles and their recontraction (O in 2c–e). Alternation in the shape of the crystallites (2e–i). Coalescence of nearby pairs of particles (A in 2f–i). Tendency to split and subsequent coalescence of these particles (M in 2g–i).	FeAl$_2$O$_4$ and a solid solution with d-values close to those of Al$_2$Fe$_2$O$_6$ when torus shape is observed. FeAl$_2$O$_4$ and a solid solution with d-values decreased from those corresponding to the case above and trace α-Fe when core-and-ring structure is observed
Table 2$_{6,500}$		
1 h	Uniform size particles with torus shape (3a).	FeAl$_2$O$_4$, traces of Al$_2$Fe$_2$O$_6$
2.5 h	Increase in size of particles. Torus shape is maintained still. Very small cores are present in cavities of particles (1.b in 3c). Disappearance of small and large particles (I in 3b, c). Disappearance of a large particle nearby a smaller particle (H in 3b, c) coalescence of nearby particles (A in 3a–c), dumbbell-shape particles (A in 3a, c), decrease in size and disappearance of some particles (D.b in 3b, c), migration and coalescence of particles (B in 3a–c), growth of some small particles (J in 3b, c) and extension and/or recontraction of particles are observed.	Increase in the intensity of Al$_2$Fe$_2$O$_6$
Up to 27 h	Marginal extension and contraction.	An increase in Al$_2$Fe$_2$O$_6$ and a decrease in FeAl$_2$O$_4$
Table 2$_{12.5,500}$		
2 h	Particles with sharp, core-and-ring structure form. Small particles have a torus shape. (4a)	Fe$_3$O$_4$(γ-Fe$_2$O$_3$), α-Fe

TABLE 2—*Continued*

Total heating time	Event observed	Compound identified
3 h	All particles acquire torus shape. Some extension, and coalescence following contact. A few small particles decrease in size or disappear.	
4 h	Particles contract. Particles acquire a core-and-ring structure. A number of small particles disappear (E in 4a, b). Coalescence of a few nearby pairs of particles (A in 4a, b).	
5 h	Formation of compact particles. Decrease in size and/or disappearance of small particles, some of which coalesce with neighbors (A, E in 4b, c). Ripening between a few particles (D.a, D.b, D.c, in 4'a–c).	Mostly α-Fe
6 h	Disappearance of some more small particles.	Almost only α-Fe
Up to 24 h in a few steps	Compact, dark particles are formed. No other change. (4d)	Almost only α-Fe
46 h (22 in one step)	Particles are considerably extended and each particle encloses a cavity. The particles appear porous. Small fragments seen in the cavities of some particles (S.a in 4e).	Solid solution of Fe_2O_3 and Al_2O_3 with d-values slightly larger than those of Fe_3O_4 (γ-Fe_2O_3)
Table $2_{6,600}$		
2 h	Particles with core-and-ring structure form. The core is smaller and the annular gap is wider than at lower temperature. (5a, c)	More of $FeAl_2O_4$ and less of Fe_3O_4 (γ-Fe_2O_3)
4 h	The particles contract and tend to form compact particles. Very little change in the number of particles.	
Up to 41 h	Alternation in shape between a core-and-ring structure and a 3-dimensional compact structure. (5b, d)	More of Fe_3O_4 (γ-Fe_2O_3), traces of $Al_2Fe_2O_6$ and α-Fe
Table $2_{6,700}$		
1 h	Very few distinct crystallites are detected. (6a)	Al_2O_3
5 h	Light (low contrast) and mostly small particles are detected. (6b)	Faint rings of α-Fe, Al_2O_3
8 h	Increase in size and darkening of all particles. (6c)	$FeAl_2O_4$, faint rings of α-Fe and Fe_3O_4 (γ-Fe_2O_3)
18 h	Growth of particles. Crystallites are dark and compact. Very little change in the number of resolved particles. (6d)	$FeAl_2O_4$
Up to 34 h	Migration (C), splitting (N), coalescence (A) and appearance of new particles (L) are detected. Traces of particle peripheries (P) and film around particles (Q) are also observed. (6e, f)	
Table $2_{6,800}$		
	(Sample previously heated at 600°C for 41 h). (7a)	

TABLE 2—*Continued*

Total heating time	Event observed	Compound identified
$2\frac{1}{2}$ h	Very dark, compact particles are formed (K). No change in the number and position of the particles. (7b)	A compound with d-values slightly greater than those of Fe$_3$O$_4$ (γ-Fe$_2$O$_3$)
4 h	Considerable sintering and rearrangement of particles is observed (F). Migration of some large crystallites detected (C). Marks of particle peripheries seen (P). (7c)	Fe$_3$O$_4$ (γ-Fe$_2$O$_3$) and Al$_2$Fe$_2$O$_6$

[a] The first subscript refers to the loading in Å and the second to the temperature in °C.
[b] The numbers in parentheses refer to the figure numbers.

Al$_2$Fe$_2$O$_6$. Thus an increase in the d values toward those of Al$_2$Fe$_2$O$_6$ indicates the formation of Fe$_2$O$_3$ and its subsequent dissolution in Al$_2$O$_3$; conversely, a decrease in the d values of one such solid solution toward those of γ-Fe$_2$O$_3$ (Fe$_3$O$_4$) indicates a partial precipitation of Fe$_2$O$_3$ from the solid solution and its eventual reduction to the metal and/or a nonstoichiometric lower oxide. In comparison to the former case, the latter can be considered a relatively reduced (less oxidized) state. The major d values of Al$_2$O$_3$ and of the lower aluminate, FeAl$_2$O$_4$, are in the order FeO > FeAl$_2$O$_4$ > Al$_2$O$_3$ and therefore, the formation of solid solutions between FeO and Al$_2$O$_3$, ultimately leading to FeAl$_2$O$_4$, can also be inferred from the increase or decrease in the d values. One may note that FeO is not stable below 560°C as a separate phase. The stoichiometric aluminates, FeAl$_2$O$_4$ and Al$_2$Fe$_2$O$_6$, have been detected in some cases. When the d values have not corresponded to the stoichiometric aluminates or oxides, solid solution formation has been inferred for reasons discussed above.

At 400°C, the total number of crystallites remained almost constant for heating times greater than 1 h. A few nearby pairs of particles coalesced following their contact because of extension (A in Figs. 2f–i). The crystallites, however, underwent alternate changes in shape from a torus enclosing a cavity to one in which an annular ring separates the torus from a core in the cavity

(Figs. 2e–i). The torus shape was found to be associated with a more oxidized state and the core-and-ring structure with a relatively less oxidized state as discussed in detail in Ref. (*22*).

At 500°C, after heating in hydrogen for 6 h, both 6- and 12.5-Å specimens exhibited stability with respect to further growth (Tables 2$_{6,500}$ and 2$_{12.5,500}$).[2] However, whereas at the lower loading almost no metal was detected in the diffraction pattern even after a total of 27 h of heating in the as-supplied hydrogen, at the higher loading almost only metal was detected after only 6 h of heating in the same as-supplied hydrogen. This shows that only samples with high metal loadings can be reduced to the zerovalent state with hydrogen. As seen from the tables, the events observed and the compounds formed indicate that the chemical interactions between the crystallites and the substrate are very strong and result in the dissolution of the metal oxide in alumina and/or of alumina in the metal oxide. It appears that for the low loading used, it is almost impossible at 400 or 500°C to obtain the zero-valent metal with the as-supplied hydrogen. Even though there is some reducibility which causes the shape alternations (*22*), it is not sufficiently large to yield detectable α-Fe. The higher loading (12.5 Å) yielded, however, compact metallic par-

[2] The first subscript refers to the initial film thickness in Å and the second to the temperature in °C.
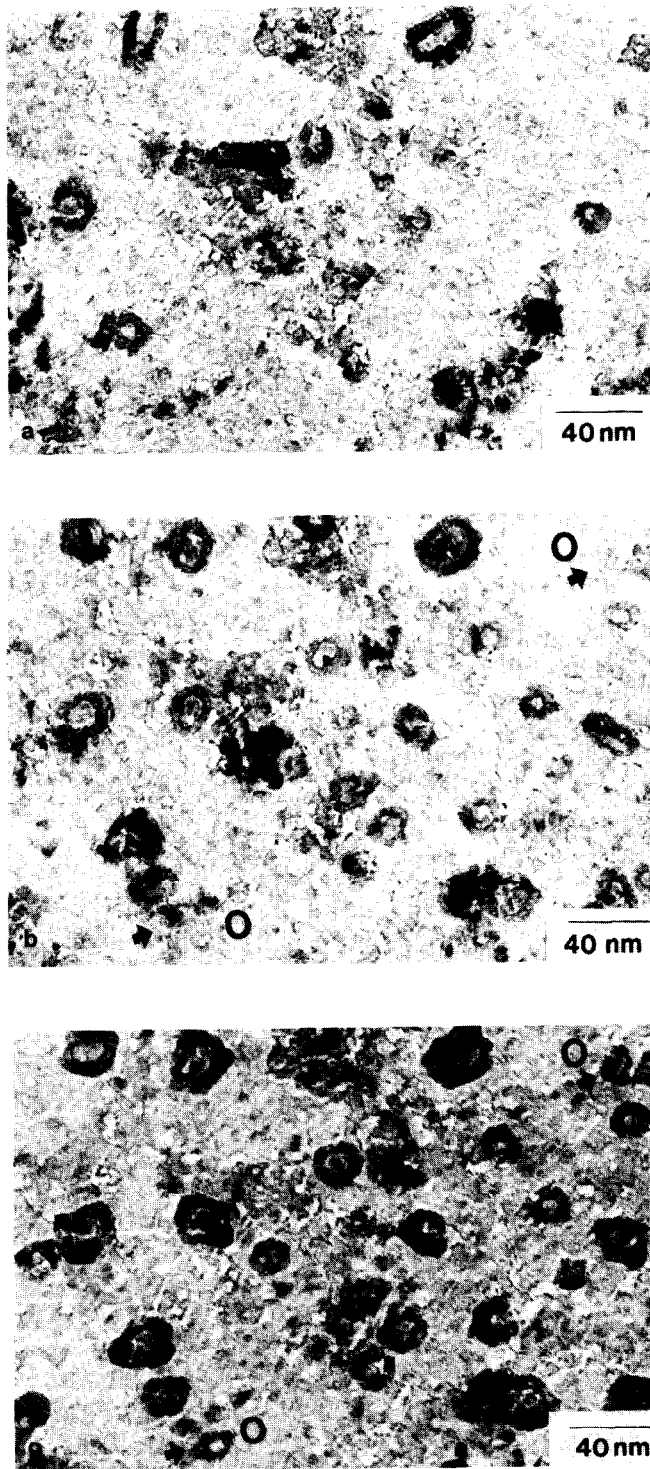
FIG. 2. Sequence of changes of a specimen heated at 400°C in as-supplied hydrogen. Initial loading, 6 Å. The micrographs show the same region after (a) $\frac{1}{2}$ h, (b) 1 h, (c), 2 h, (d) 3 h, (e) 6 h, (f) 12 h, (g) 21 h, (h) 33 h, (i) 36 h.
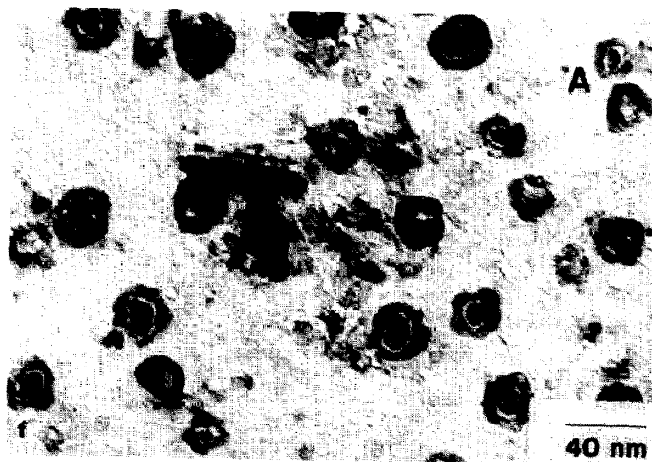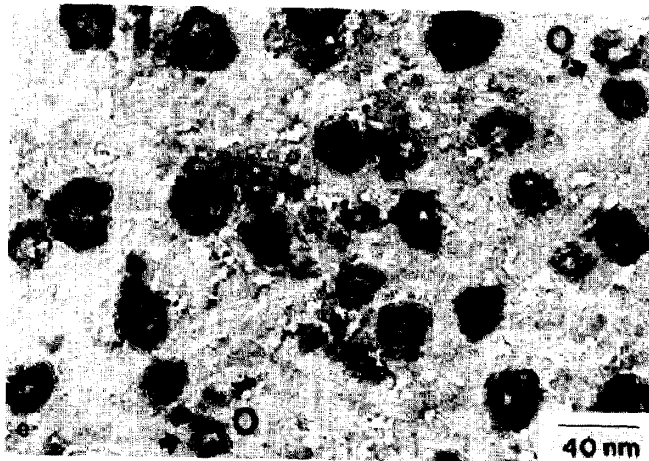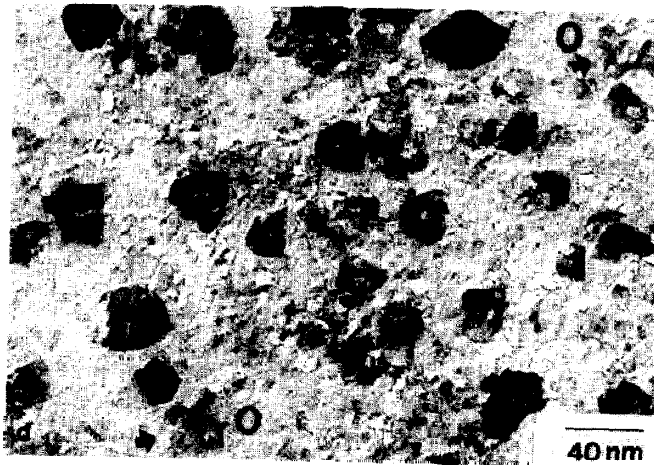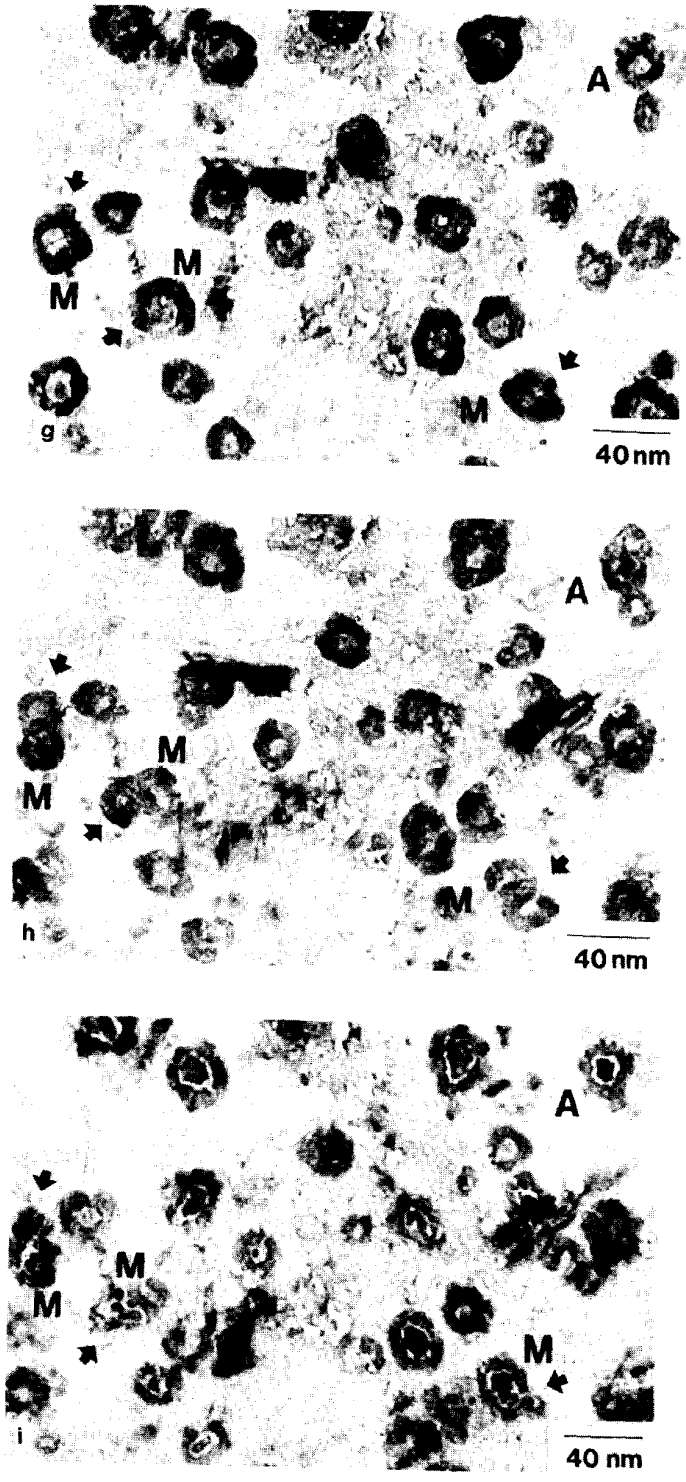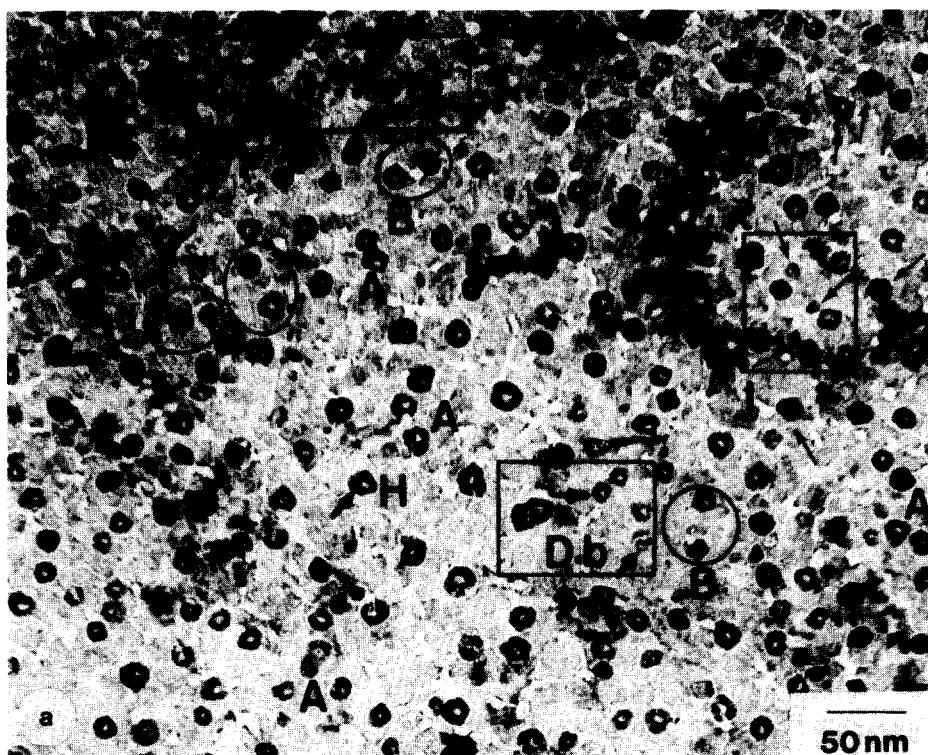
FIG. 2—*Continued.*

FIG. 2—*Continued*.

FIG. 3. Time sequence of the same region of the specimen heated previously at 300°C on subsequent heating in as-supplied hydrogen at 500°C. (a) 1 h, (b) 2 h, and (c) 5 h.

ticles of α-Fe which subsequently sintered considerably.

The results at 600°C for a loading of 6 Å are listed in Table 2$_{6,600}$. Unlike at lower temperatures, the crystallites alternated in shape between a core-and-ring structure and a three-dimensional, compact structure, instead of a torus (Figs. 5a–d). At this temperature and loading, the compact structure is associated with FeAl$_2$O$_4$, Fe$_2$O$_3$, and only traces of α-Fe. In contrast, at 500°C and 12.5-Å loading, the compact particles were associated mostly with α-Fe.

Distinct crystallites formed more slowly at 700°C (Table 2$_{6,700}$) than at 400 to 600°C (Table 2$_{6,400}$–2$_{6,600}$). Distinct crystallites could not be detected after an initial heating for 1 h (Fig. 6a). In addition, only rings of Al$_2$O$_3$ were present in the diffraction pattern. Possibly, very thin particles were present in an oxidized extended form on the substrate, undetectable by TEM and elec-

tron diffraction. The same observation is also valid for the 300°C treatment. At the lower temperature of 300°C, after about 2 h of heating the iron oxide molecules of the small (not well formed) clusters probably diffused into the substrate to form aluminate. At the higher temperature of 700°C, they are perhaps present initially as large, extended, thin islands of oxide, or even aluminate, too thin to be detected by electron diffraction. During the initial few hours of heating, the rate of aluminate formation is probably faster at 300°C than at 700°C because a larger fraction of molecules is in contact with alumina in the former than in the latter case. (In addition, since the clusters may not be well formed at 300°C, the molecules may be loosely held to one another.) The subsequent increase in size and contrast, with the number of crystallites remaining almost the same (Table 2$_{6,700}$, Fig. 6c), occurs probably as a result of coales-
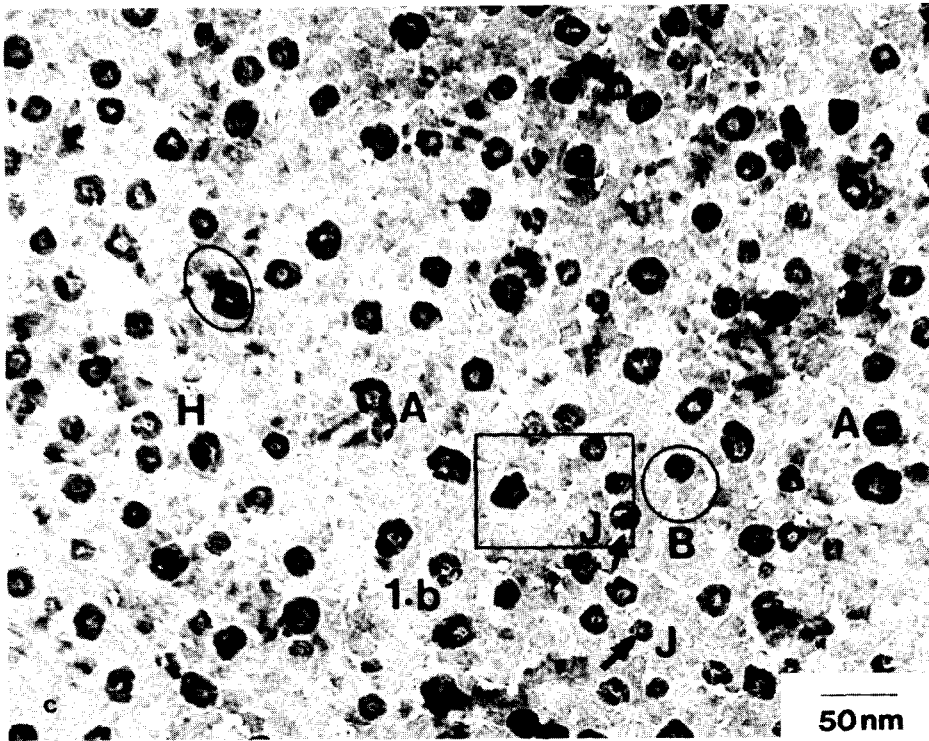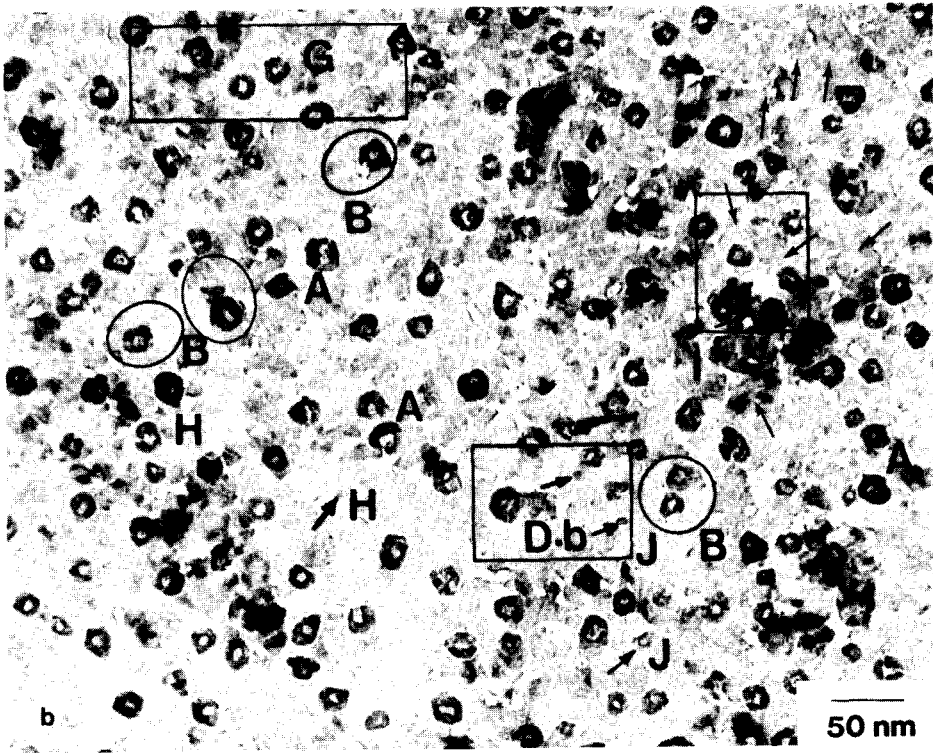
FIG. 3—*Continued.*

TABLE 3

Alternate Heating in Hydrogen and Oxygen

Heating atmosphere	Event observed	Compound identified
Table 3$_{6,400}$		
O$_2$	Torus shape particles with a tendency to fill in the cavity of the torus are observed.	Fe$_3$O$_4$ (γ-Fe$_2$O$_3$), Al$_2$Fe$_2$O$_6$
H$_2$	Particles acquire the core-and-ring structure. Coalescence of nearby particles and rupture of some particles are seen.	FeAl$_2$O$_4$, α-Fe
Table 3$_{6,500}$		
O$_2$	Considerable filling in of the cavities of the torus. Some pairs of neighboring particles make contact following extension. (8c)	Al$_2$Fe$_2$O$_6$, Fe$_3$O$_4$ (γ-Fe$_2$O$_3$), trace FeAl$_2$O$_4$
H$_2$	Particles acquire a core-and-ring structure initially but on continued heating assume a torus shape. Particles in contact coalesce. (8a, b, d, e)	Fe$_3$O$_4$ (γ-Fe$_2$O$_3$), trace FeAl$_2$O$_4$
Table 3$_{12.5,500}$		
O$_2$	Extension. Tendency to fill in the cavity. Coalescence of nearby particles. Particles composed of loosely interconnected units. (9a, d, e, f; 10b)	d-Values approaching those of Al$_2$Fe$_2$O$_6$ and FeAl$_2$O$_4$
H$_2$	Splitting of particles into a few interconnected sub-units, a few of which coalesced subsequently (V). Periphery marks seen around particles (P). Fragmentation of particles (W). (9b, c, g; 10a, c, d)	α-Fe, traces of Fe$_3$O$_4$ (-Fe$_2$O$_3$)
Table 3$_{6,600}$		
O$_2$	(Sample was previously heated in hydrogen at 800°C for 4 h, Fig. 7c). Migration of some particles (C). A film appears to extend out from underneath and around the particles. (11a, b)	Fe$_3$O$_4$ (γ-Fe$_2$O$_3$), Al$_2$Fe$_2$O$_6$, traces of FeAl$_2$O$_4$
H$_2$	Contraction and formation of more circular particles. Periphery marks, observed before, contract to form small particles (X). (11c)	Mostly Fe$_3$O$_4$ (γ-Fe$_2$O$_3$), traces of FeAl$_2$O$_4$, traces of α-Fe
Table 3$_{6,700}$		
O$_2$	A thick film extends from the periphery of the particles. Considerable extension or disappearance of small particles (E). Substrate grain boundaries appear less sharp (R). Very little extension of large particles. (12b, c)	Mostly FeAl$_2$O$_4$ and some Fe$_3$O$_4$ (γ-Fe$_2$O$_3$)
H$_2$	Appearance of a few, new, small particles (L). (12d)	FeAl$_2$O$_4$

cence of the unresolved extended islands with the nearby resolved particles or by ripening. After a total of 18 h of heating, almost only FeAl$_2$O$_4$ is detected. The fact that only aluminate is detected indicates that, perhaps, it is present not only in the substrate, but on its surface and also in as well as on the particles.

A.2. Alternate heating in oxygen and as-supplied hydrogen. Heating in oxygen caused, in general, extension of the crystal-lites over the substrate, as seen from Table 3. In addition, in the oxidized and extended state, the crystallites appear to be composed of a number of very small units held together (Figs. 8c, 9e, f). Except for the coalescence of a few nearby pairs of particles following their contact, as a result of extension on oxidation, the number of crystallites remained, in general, constant during alternate heating in oxygen and hydrogen. Heating in hydrogen following heating
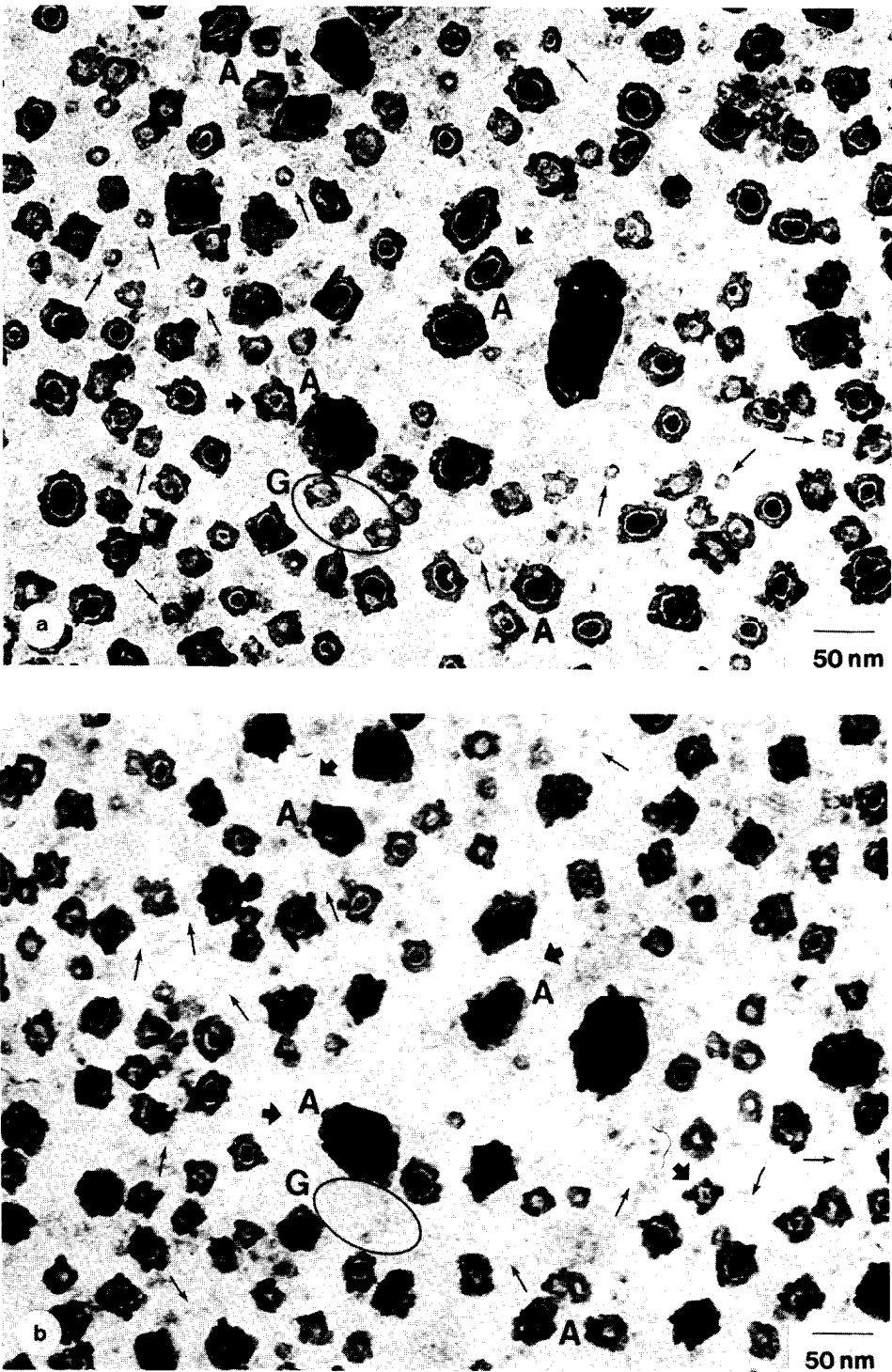
FIG. 4. Sequence of changes at 500°C in a specimen with higher loading. Initial loading, 12.5 Å. Two adjacent regions (Figs. 4 and 4′) are shown after (a) 2 h, (b) 4 h, (c) 5 h, (d) 24 h, and (e) 46 h.
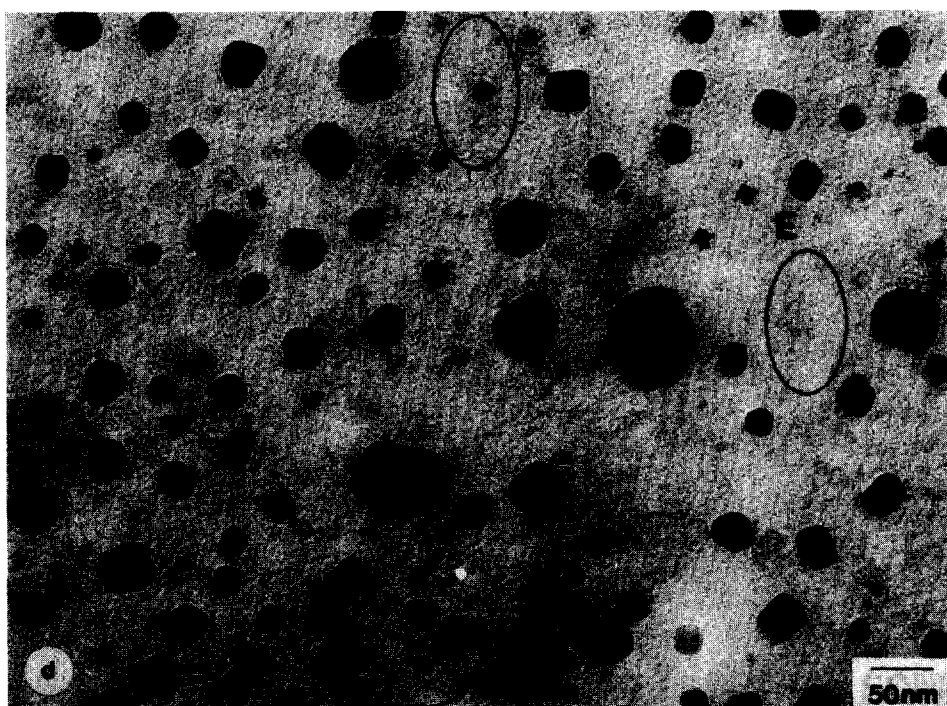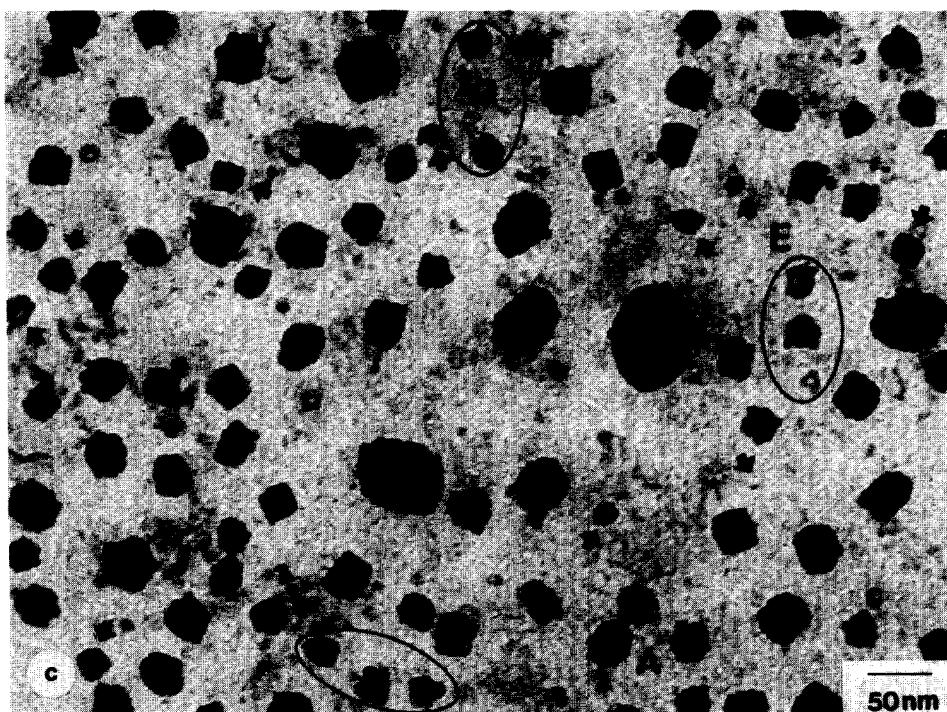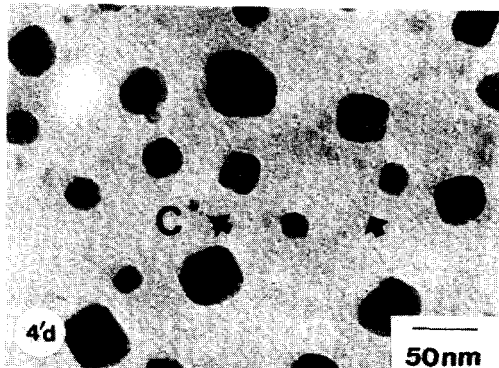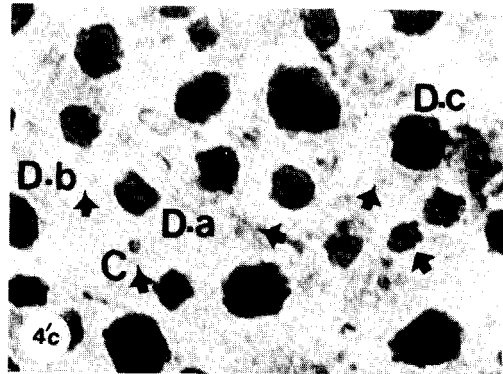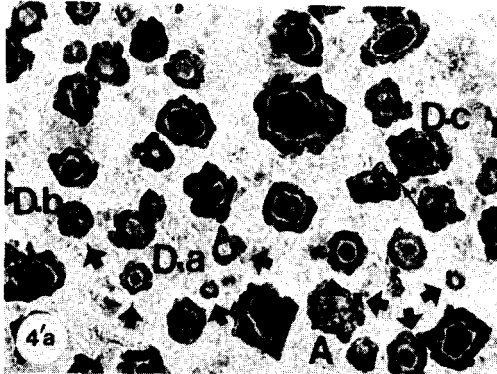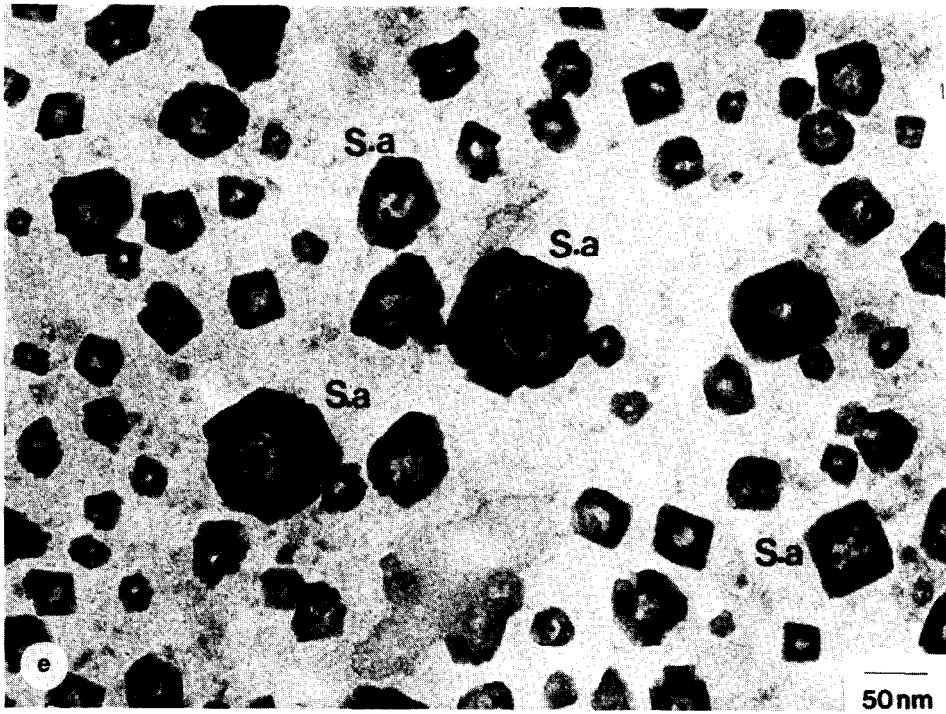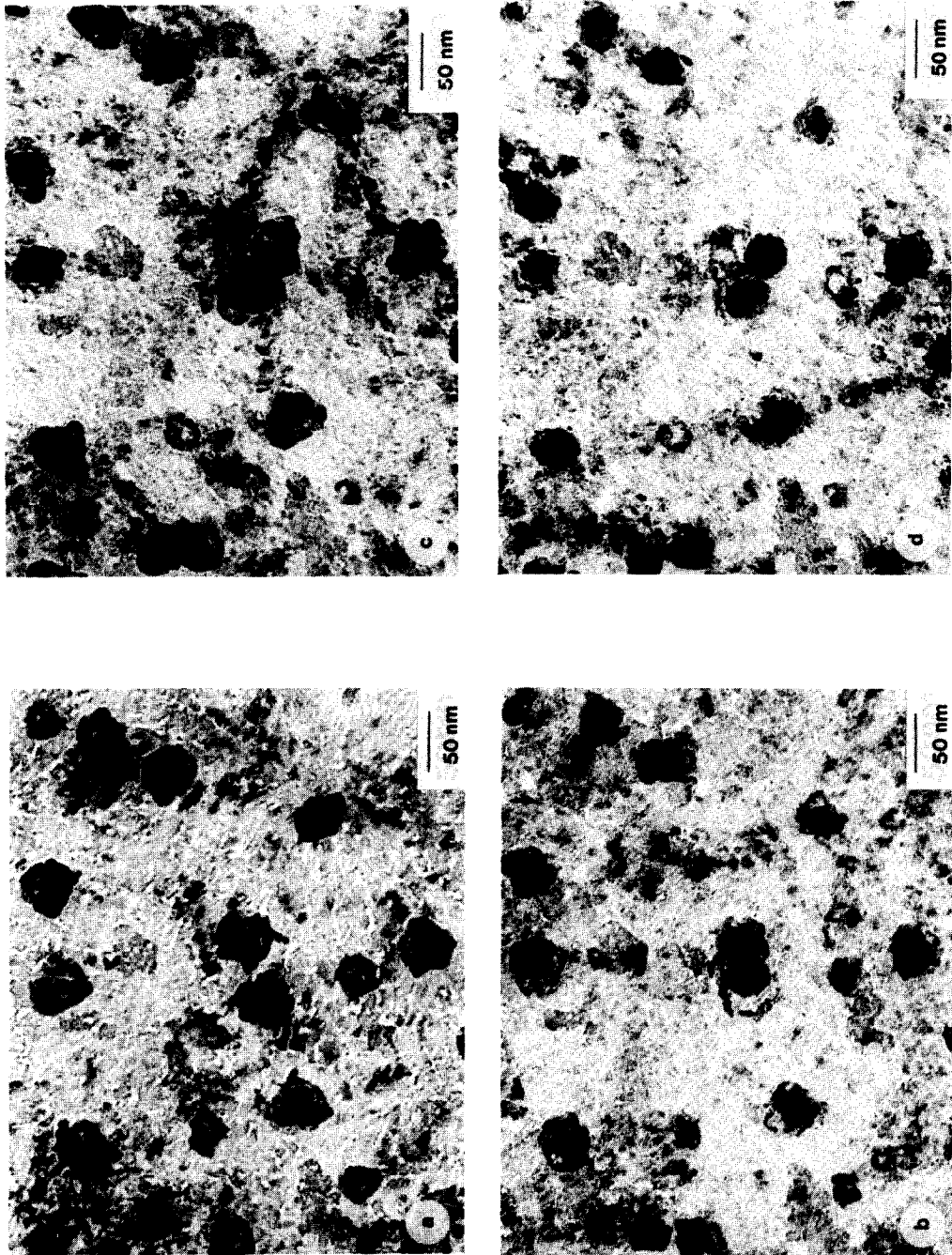
FIG. 4—*Continued.*

FIG. 4—Continued.

FIG. 5. Sequence of changes on heating a 6-Å initial loading specimen in as-supplied hydrogen at 600°C. (a) 2 h, (b) 6 h, (c) 14 h, (d) 30 h.
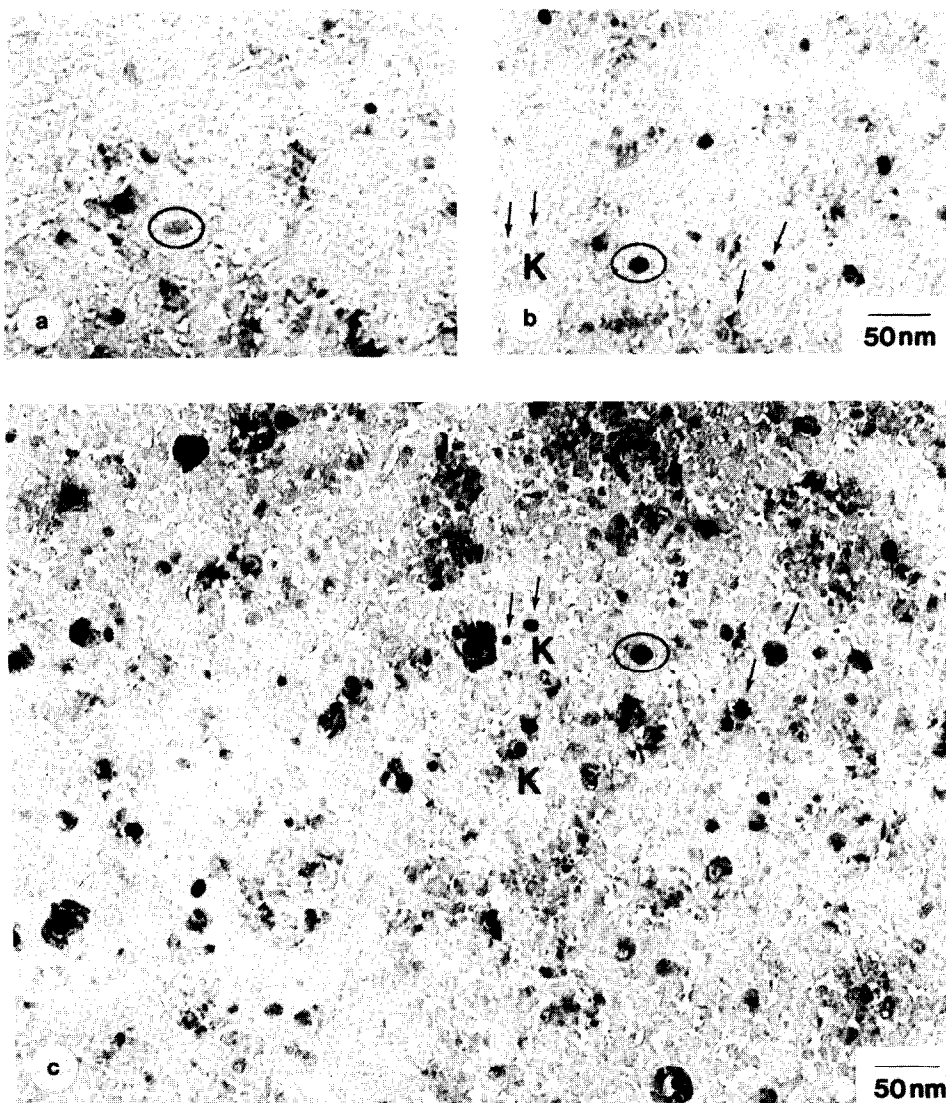
FIG. 6. Sequence of changes on heating in as-supplied hydrogen at 700°C. Initial loading, 6 Å. The same region is shown after (a) 1 h, (b) 5 h, (c) 8 h, (d) 18 h, (e) additional 3 h at 500°C (21 h total), (f) 34 h, 700°C.

in oxygen caused the particles to contract and, at 400 and 500°C, to acquire the core-and-ring structure (Table $3_{6,400}$, $3_{6,500}$).

The 12.5-Å sample exhibited interesting behavior on alternate heating in oxygen and hydrogen at 500°C. As shown in Table $3_{12.5,500}$, the crystallites extended on oxidation and split into a few interconnected particles on subsequent heating in hydrogen (Figs. 9b; 10a–d). However, the subunits coalesced and contracted to form again compact particles (Fig. 9c) on continued heating. Marks of particle peripheries could be seen in the same figure, indicating extensive interaction with the substrate along the peripheries of the particles. The crystallites extend again on heating in oxygen and cover the area bounded by the periphery marks mentioned above. In the extended state, the crystallites appear to be very po-
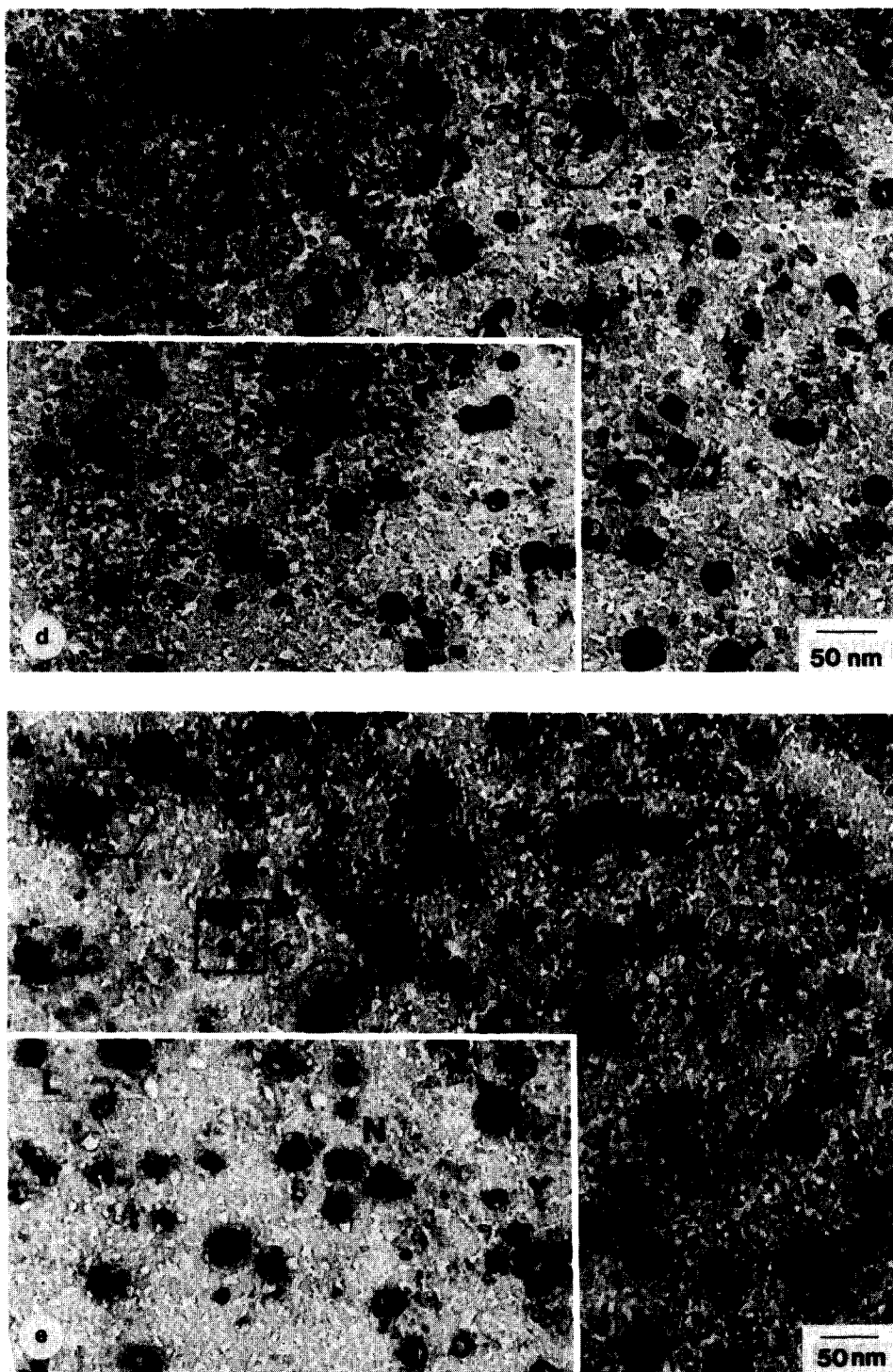
FIG. 6—*Continued.*
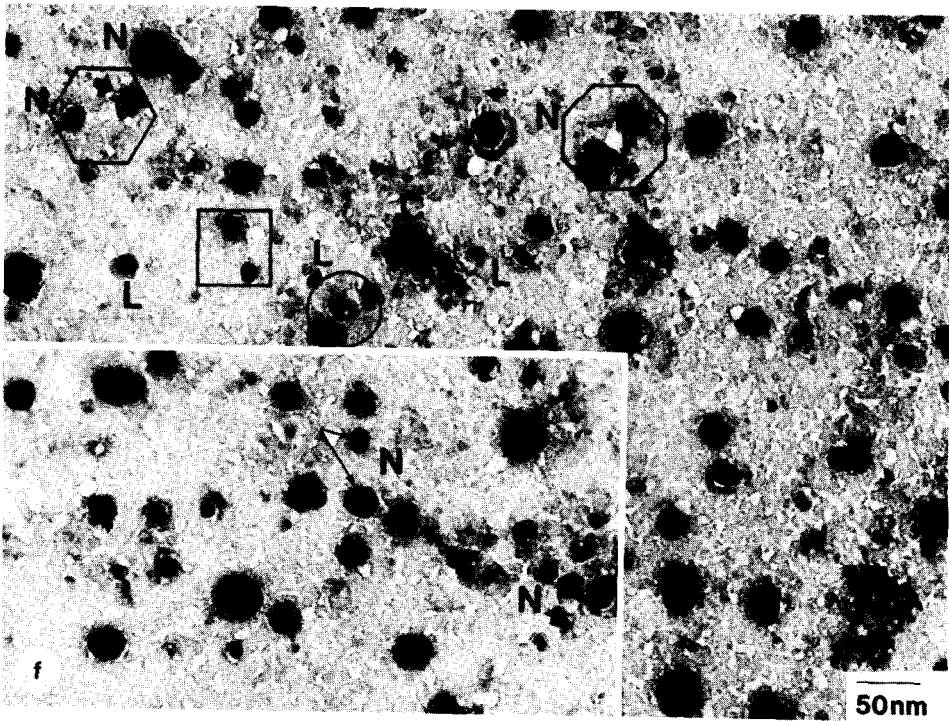
FIG. 6—*Continued.*
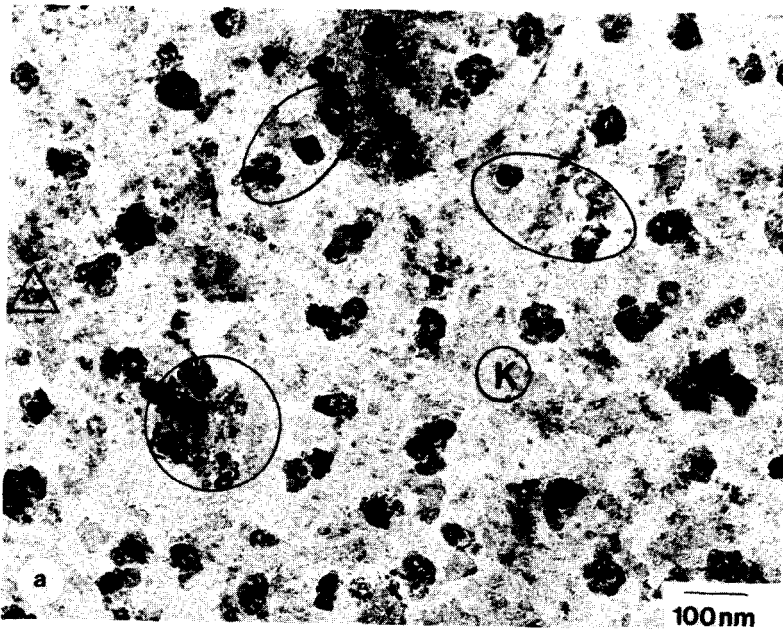
FIG. 7. Sequence of changes on heating the specimen of Fig. 5 at 800°C. The micrographs correspond to the same region: (a) 41 h, 600°C (included for reference) (b) 2 h 30 min, 800°C; (c) 4 h, 800°C.
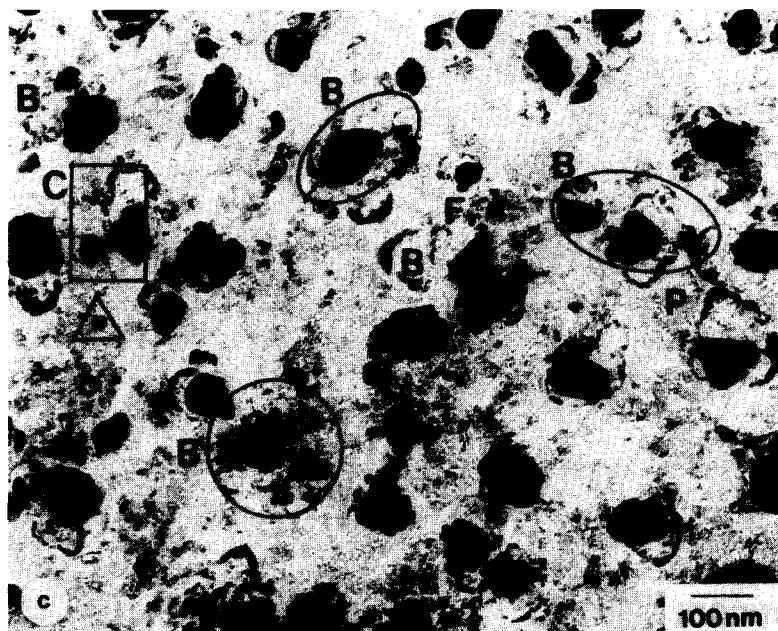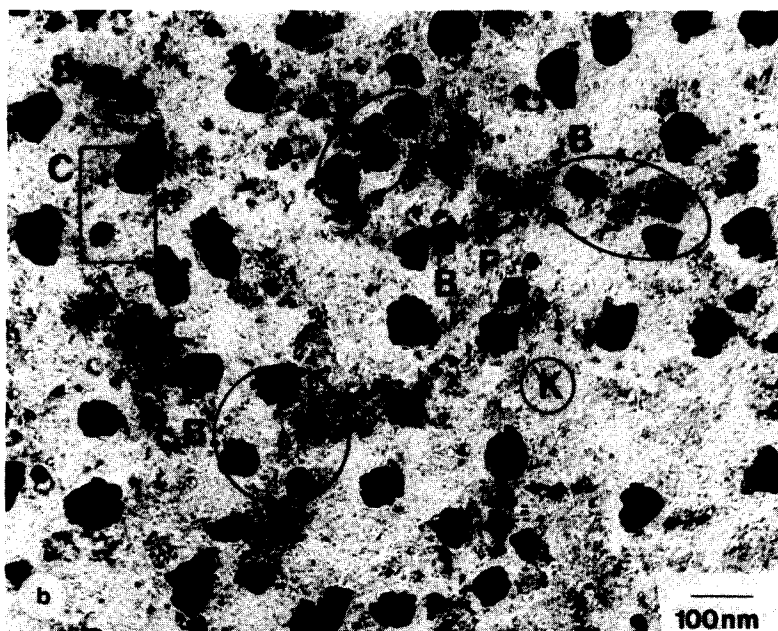
FIG. 7—*Continued.*

rous and are composed of a large number of smaller particles held together. Also, the substrate is covered with a very large number of small and thin crystallites seen clearly in a magnified micrograph (Fig. 9f). Subsequent heating in hydrogen causes the particles to contract and appear distinct, accentuating the fragmentation. The micrograph appears as if a kind of explosive shattering of the particles had occurred (Fig. 9g). In fact, the breakup occurs during heating in oxygen, as a result of the consider-
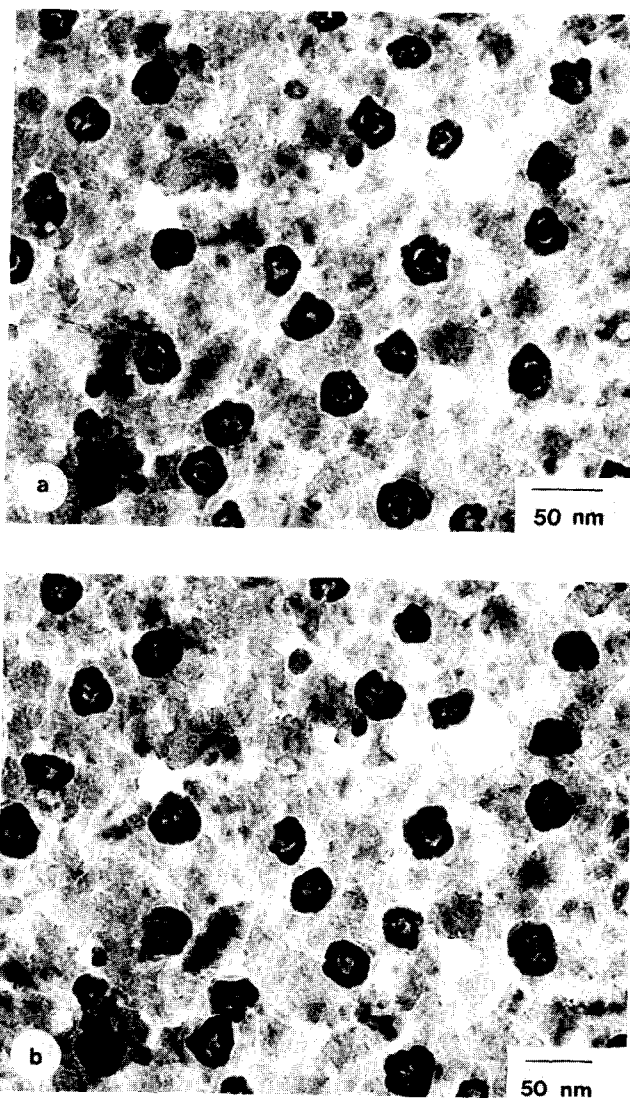
FIG. 8. Sequence of changes in the specimen of Fig. 3 on subsequent alternate heating in oxygen and hydrogen at 500°C. The region shown here is from the same specimen but of a different region than that of Fig. 3. The substrate is thicker in this region probably as a result of tearing and folding upon itself, initially. The particles are larger and the changes are sharper. The micrographs included show the changes subsequent to an oxidation step. (a) 5 h, H_2; (b) 10 h, H_2; (c) 10 h, O_2; (d) 10 min, H_2; (e) 16 h, H_2. The behavior is similar at 400°C.

able extension which, in addition, probably occurs very rapidly causing the rupture. Mechanical fatigue might have also contributed to the fragmentation since the specimen had already been heated for about 200 h.

On heating in oxygen at 700°C (Table $3_{6,700}$), a thick film extends out from the periphery of the larger particles and also the grain boundaries of the substrate appear less distinct (Figs. 12b, c). The substrate might be covered by a film. In the same micrograph, a number of small particles have disappeared (E). It is possible that both the crystallites that disappeared as well as some unresolved ones are present considerably extended on the surface covering the substrate as a thin film which co-

Fig. 8—*Continued.*

FIG. 9. Sequence of changes on heating the specimen of Fig. 4e alternately in oxygen and hydrogen at 500°C. (a) 2 h, O_2; (b) 2 h, H_2; (c) 66 h, H_2; (d) 1 h, O_2; (e) 40 h, O_2, an adjacent region; (f) magnified micrograph of (e); (g) 45 min, H_2.

TABLE 4

Heating in Purified Hydrogen

Total heating time[a]	Event observed	Compound identified
400°C, 4 h	Particles with very sharp core-and-ring structure and a broad size distribution are formed. Cores in some big particles have fringes indicating twinning (x, y in Fig. 13a). Smaller crystallites have a torus shape.	Fe_3O_4 (γ-Fe_2O_3) α-Fe
500°C, 2 h	Dark, compact particles are formed. Extremely narrow annular rings are still detected. Considerable sintering has occurred. A number of small and large particles disappeared (I). Also, a number of smaller crystallites appeared in other places (L). Coalescence of nearby particles (A) and disappearance of a large particle nearby an unaffected smaller particle (H) are detected (13a, b).	α-Fe
600°C, 4 h	Particles contract. Circular and restructured particles are formed. (13c)	α-Fe, traces of Fe_3O_4 (α-Fe_2O_3)
700°C, 2 h	Disappearance of some small particles, appearance of new ones (L), splitting (M), coalescence (A) and migration (B, C) are observed. (13d)	α-Fe

[a] 7.5 Å, progressive heating.

FIG. 9—*Continued.*
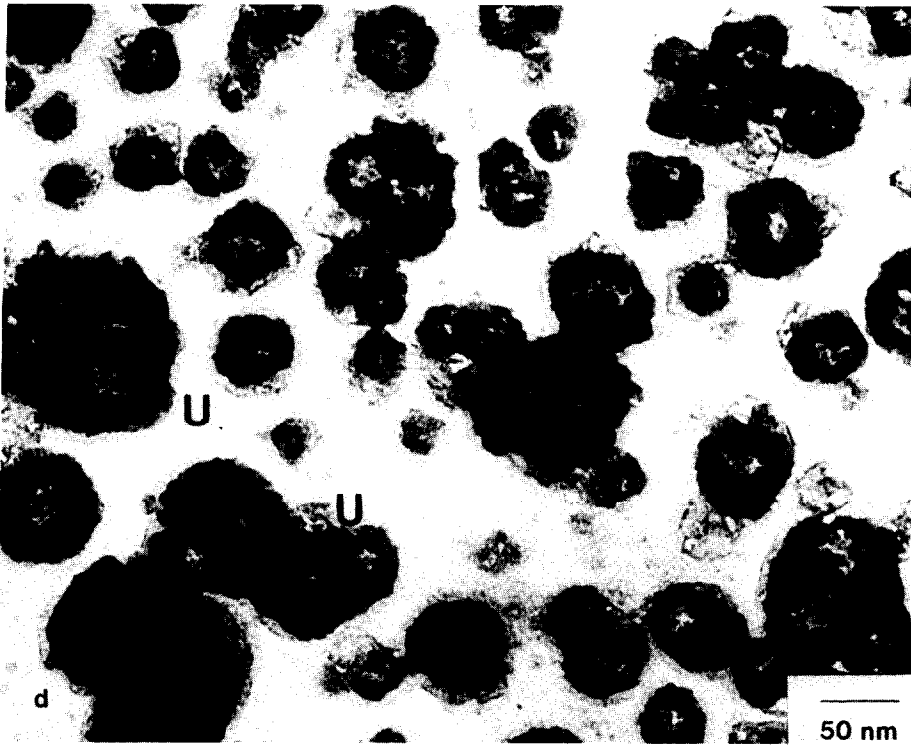
FIG. 9—*Continued.*
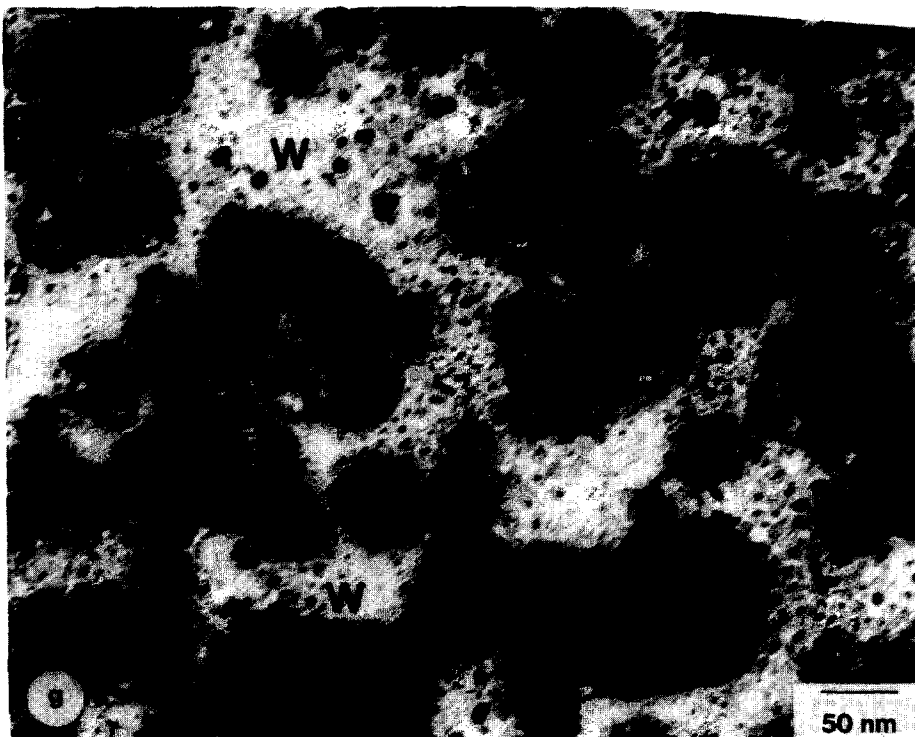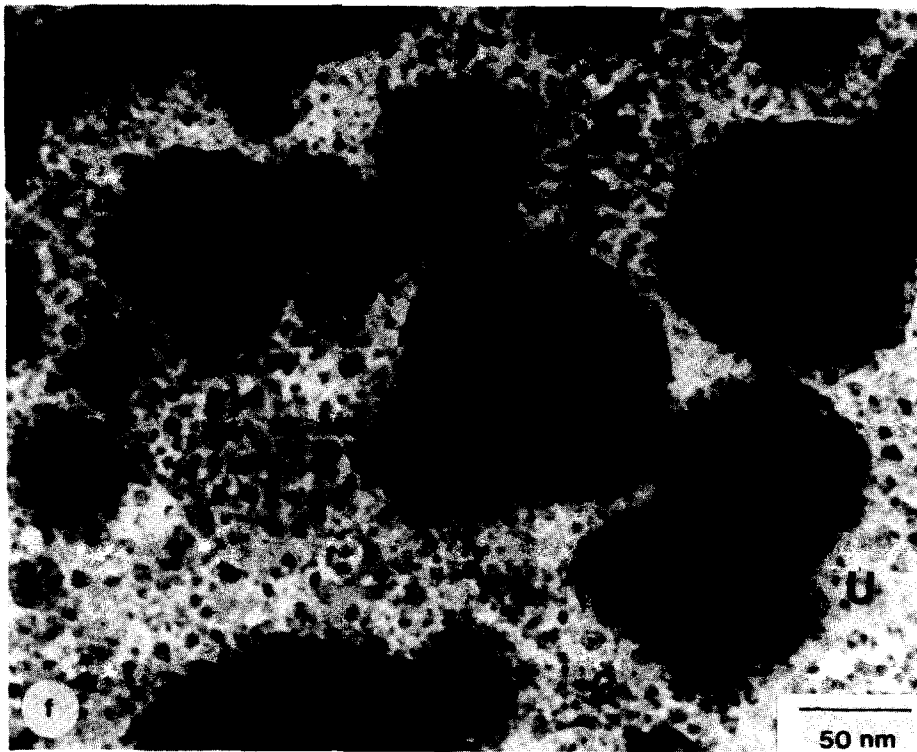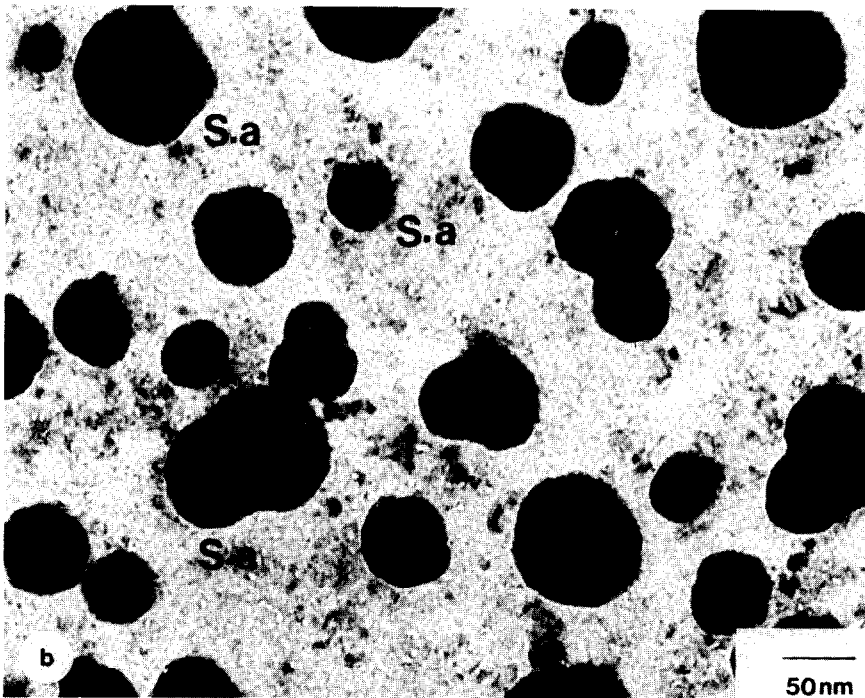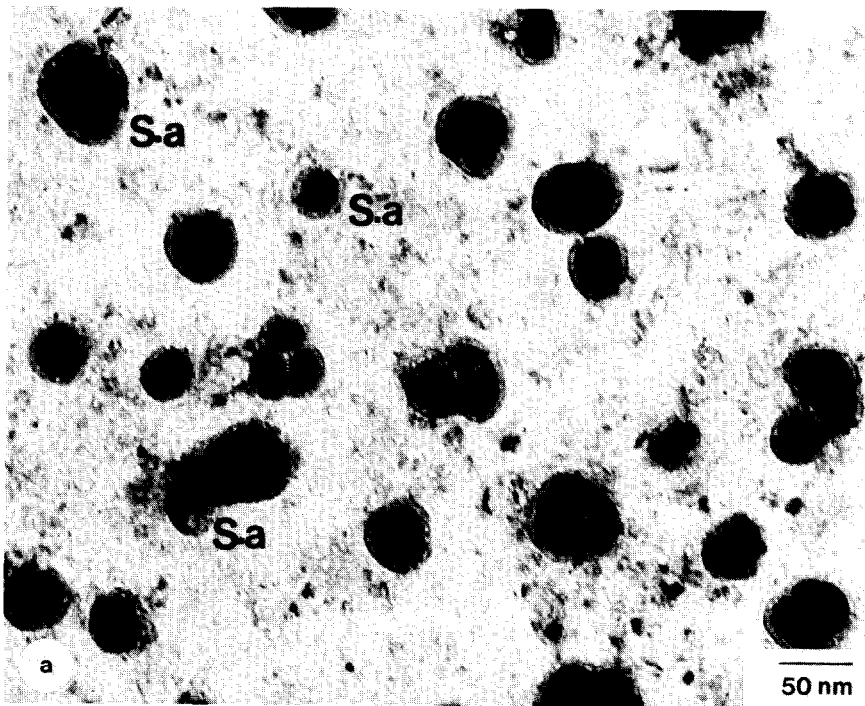
FIG. 9—*Continued.*

FIG. 10. As Fig. 9 but a different region of the same specimen better indicating the crystallite splitting. (a) 2 h, H_2; (b) 1 h, O_2; (c) 1 h, H_2; (d) 2 h, H_2.
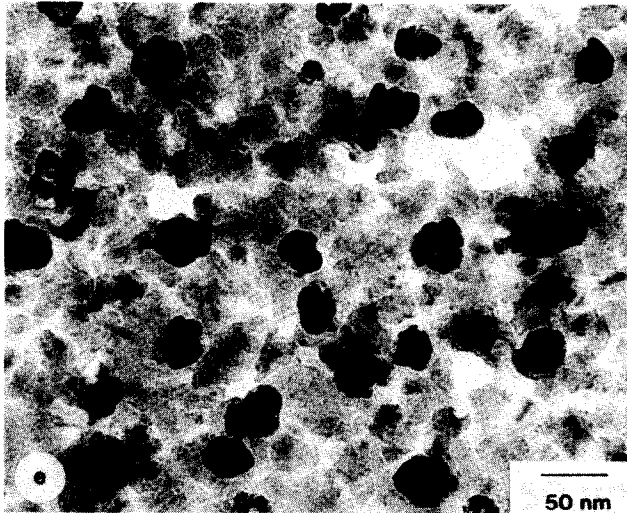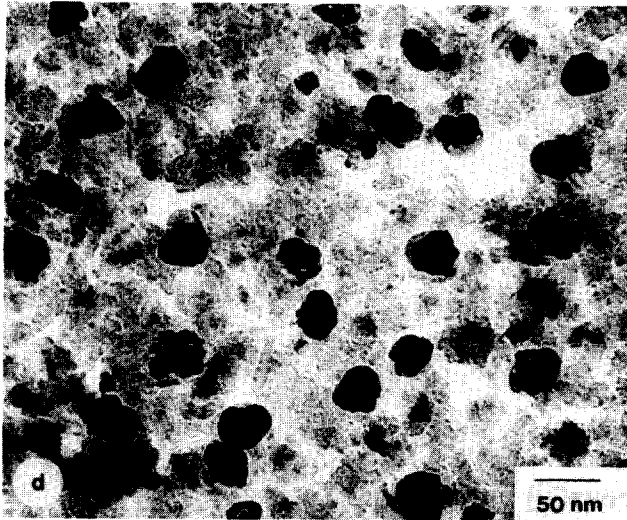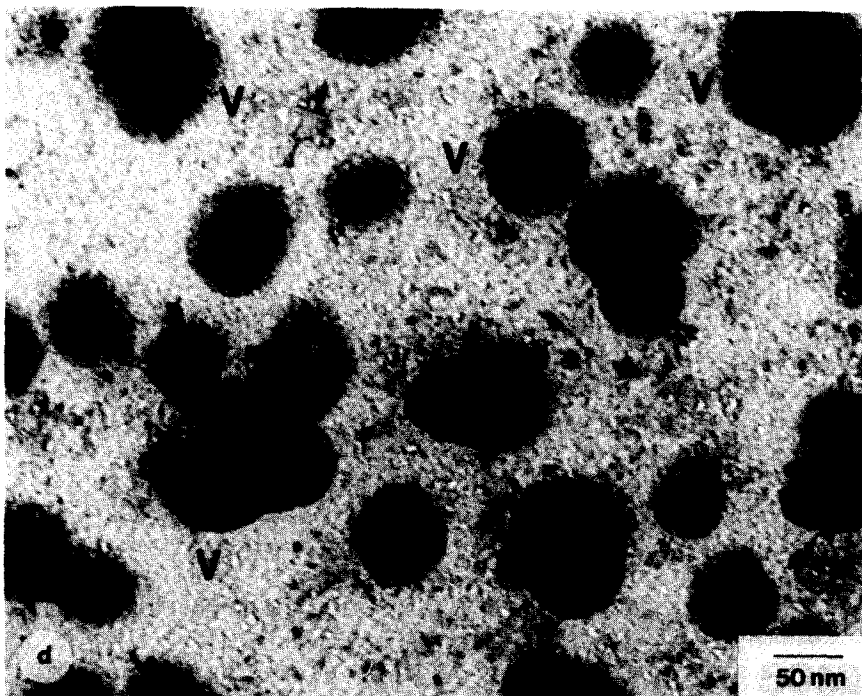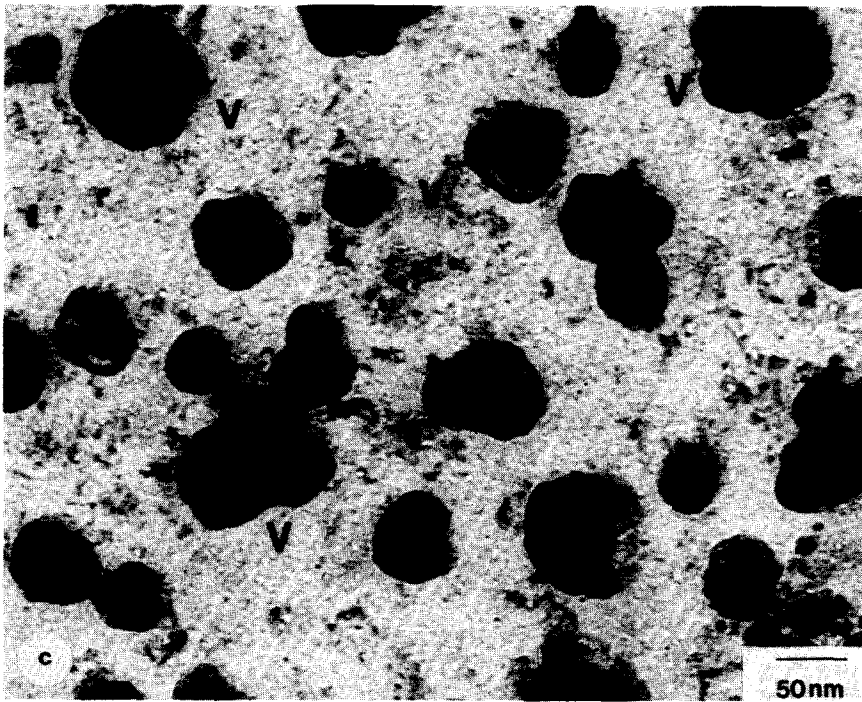
FIG. 10—*Continued.*
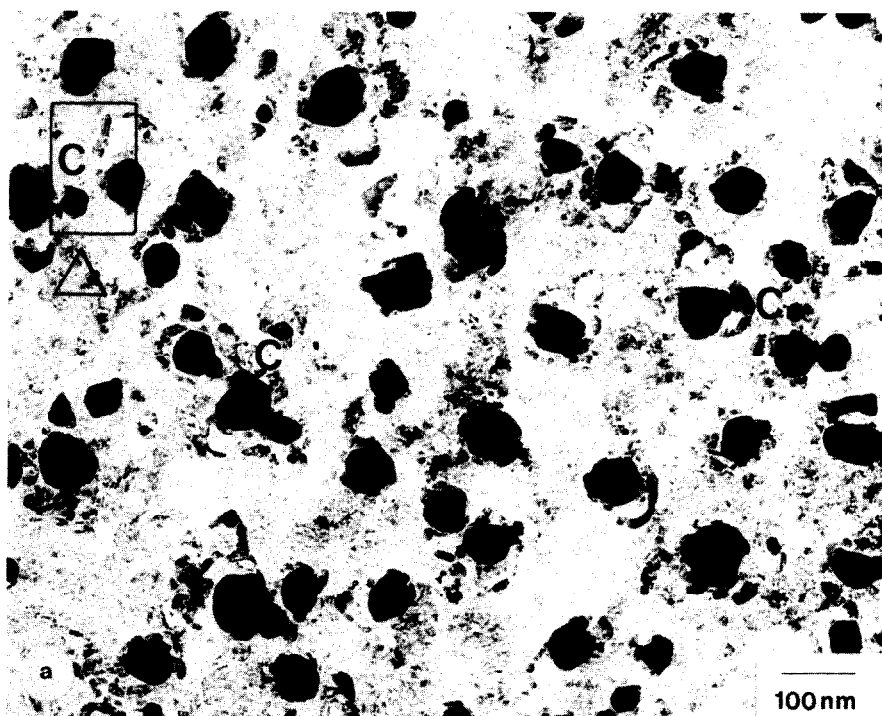
FIG. 11. Time sequence of changes on heating the specimen of Fig. 7c alternately in oxygen and hydrogen at 600°C. (a) $\frac{1}{2}$ h, O_2; (b) $1\frac{1}{2}$ h, O_2; (c) 1 h, H_2.

exists with the three-dimensional crystallites. The thin film which appears to cover the substrate might be an oxide, or more likely, an aluminate, since almost only $FeAl_2O_4$ is detected in the diffraction pattern.

B. Behavior in Purified Hydrogen

B.1. Heating in hydrogen. The behavior of the specimens when heated in purified hydrogen was different in a few respects from that observed with as-supplied hydrogen (Sect. A.1). Unlike the previous case, the initially formed crystallites are typically larger and have a bimodal distribution. Some of these initial particles are so thin that the substrate grain boundaries can be seen through them (a–c in Fig. 13a). The particles, especially the large ones, seem to prefer predominantly rectangular shapes to the usual circular ones. The events observed on heating a 7.5-Å initial film in purified hydrogen at progressively higher tem-

peratures are listed in Table 4. Metallic iron is very clearly detected even at 400°C. At 500°C and higher temperatures almost only iron is detected, with trace quantities of oxide. In contrast, with the as-supplied hydrogen the metal could not be detected even at 700°C. In addition, at 500°C and even at low loadings, relatively compact particles formed, unlike heating in the as-supplied hydrogen which led to torus-shape particles. These results point out that the difficulty in reducing the iron catalysts to the metallic state is clearly a result of the chemical interactions with the support which are caused to a considerable extent by the oxygen and/or moisture present in the reducing chamber. The micrographs (Figs. 13a, b) show that a number of particles of about 100 Å and also a few particles considerably larger (about 350 Å) disappear (H) and, instead, a number of small crystallites of about 30 Å or less appear in all the regions, including locations where no particles were
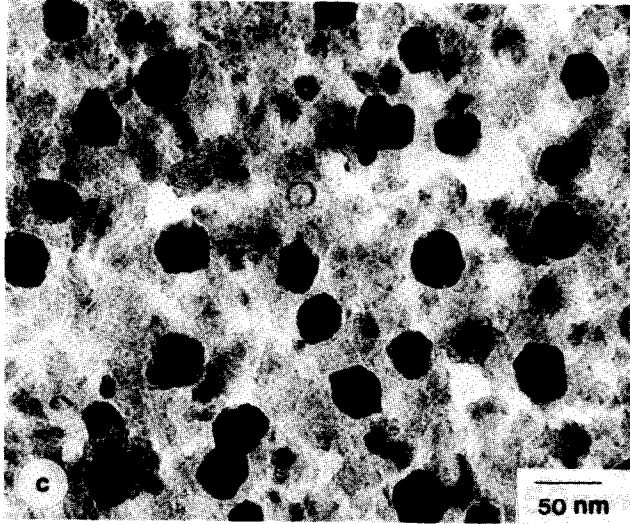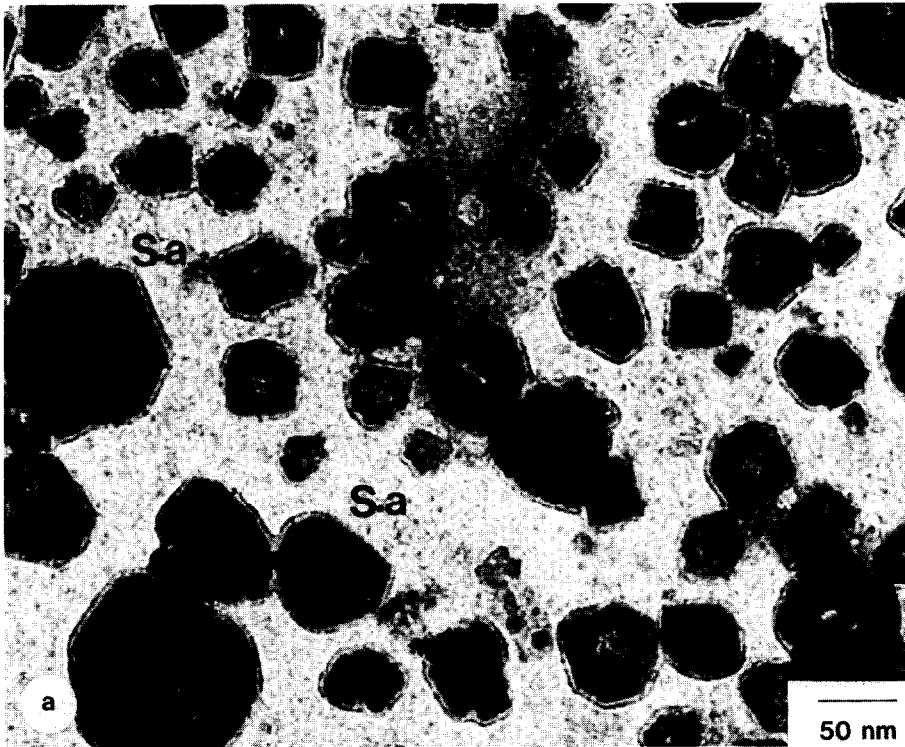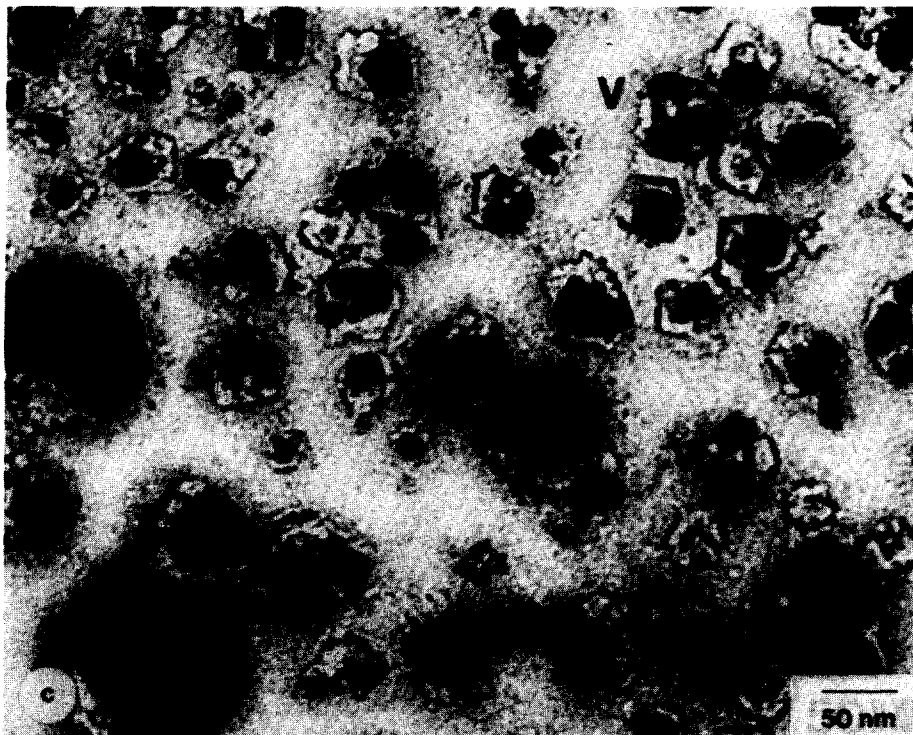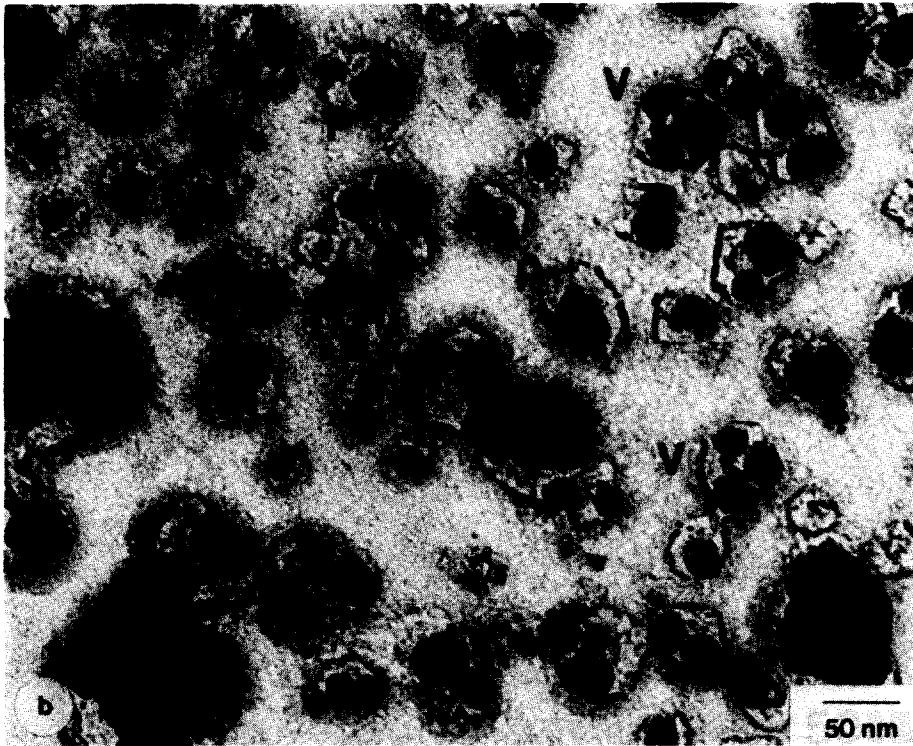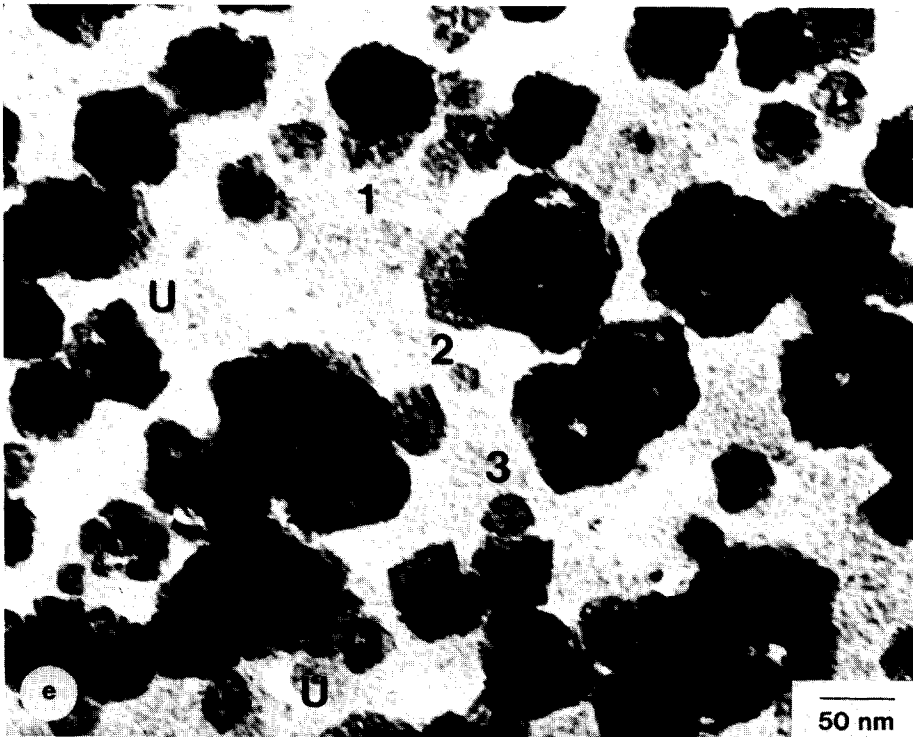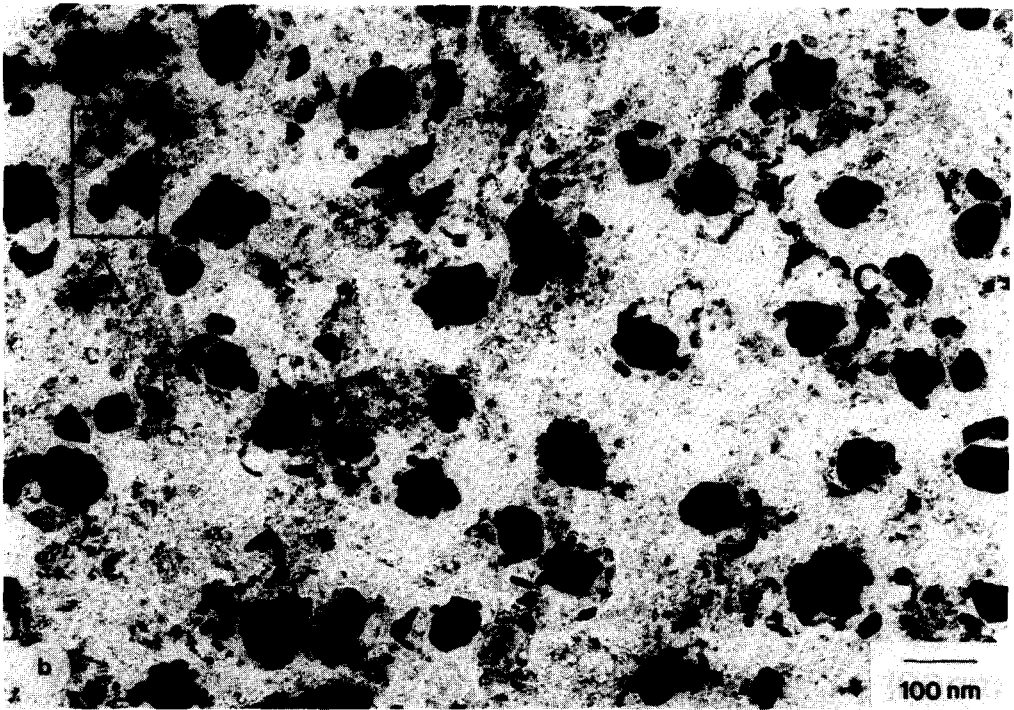
FIG. 11—*Continued.*
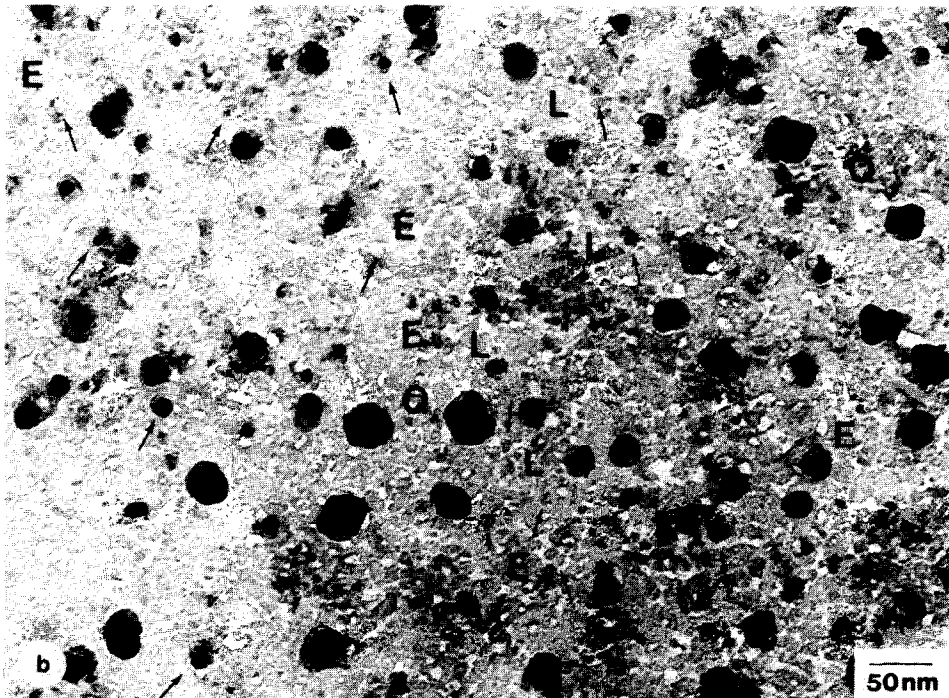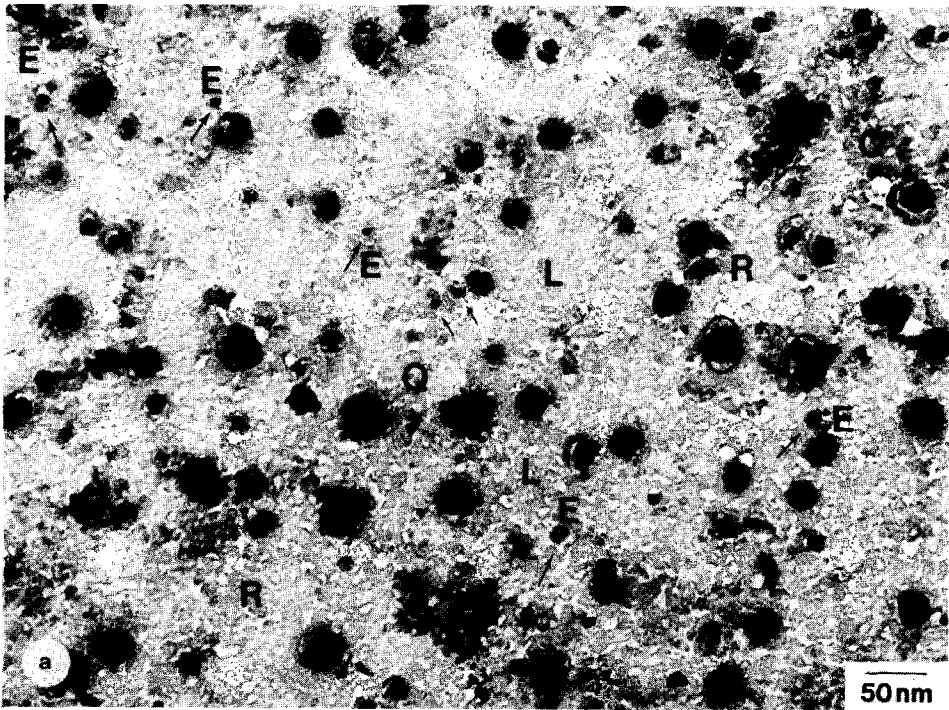
FIG. 12. Sequence of changes on heating the specimen of Fig. 6f alternately in oxygen and hydrogen at 700°C. (a) 33 h, H_2; (b) 1 h, O_2; (c) 13 h, O_2; (d) 1 h, H_2.
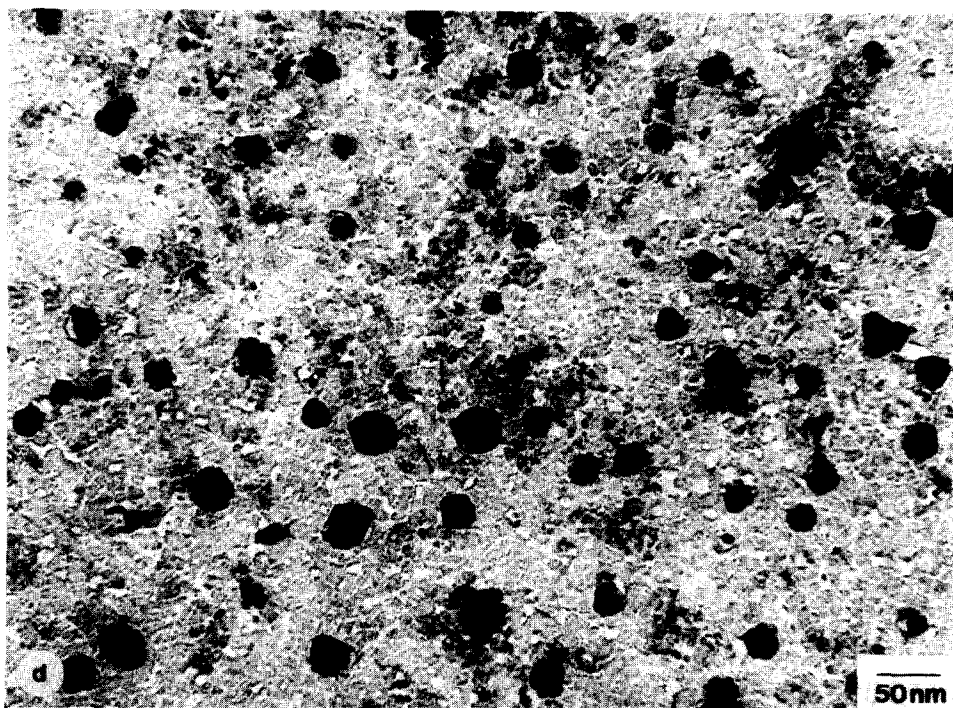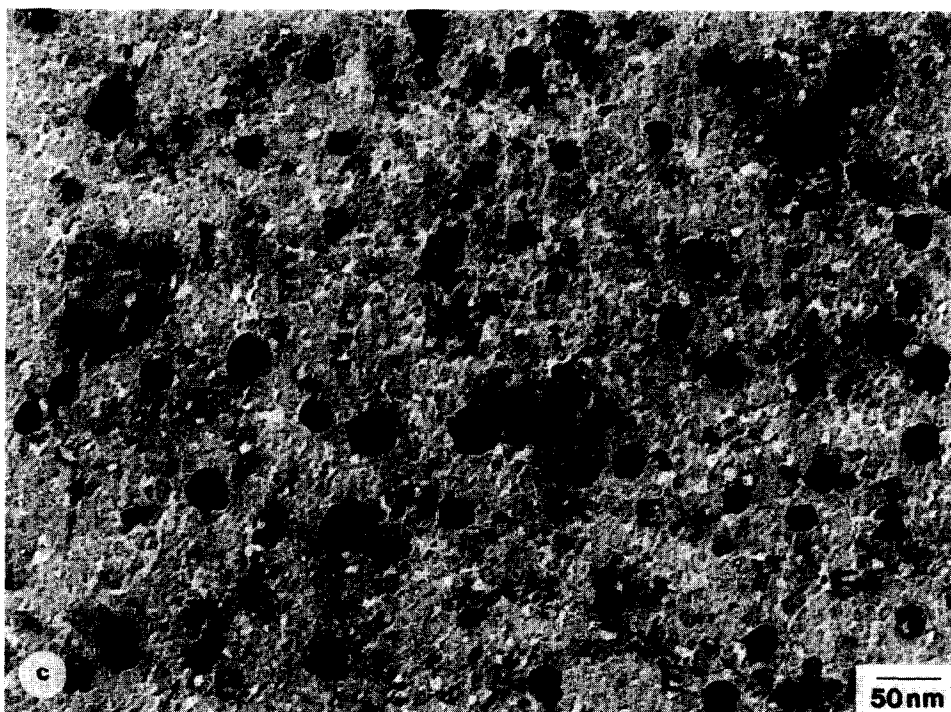
FIG. 12—*Continued.*
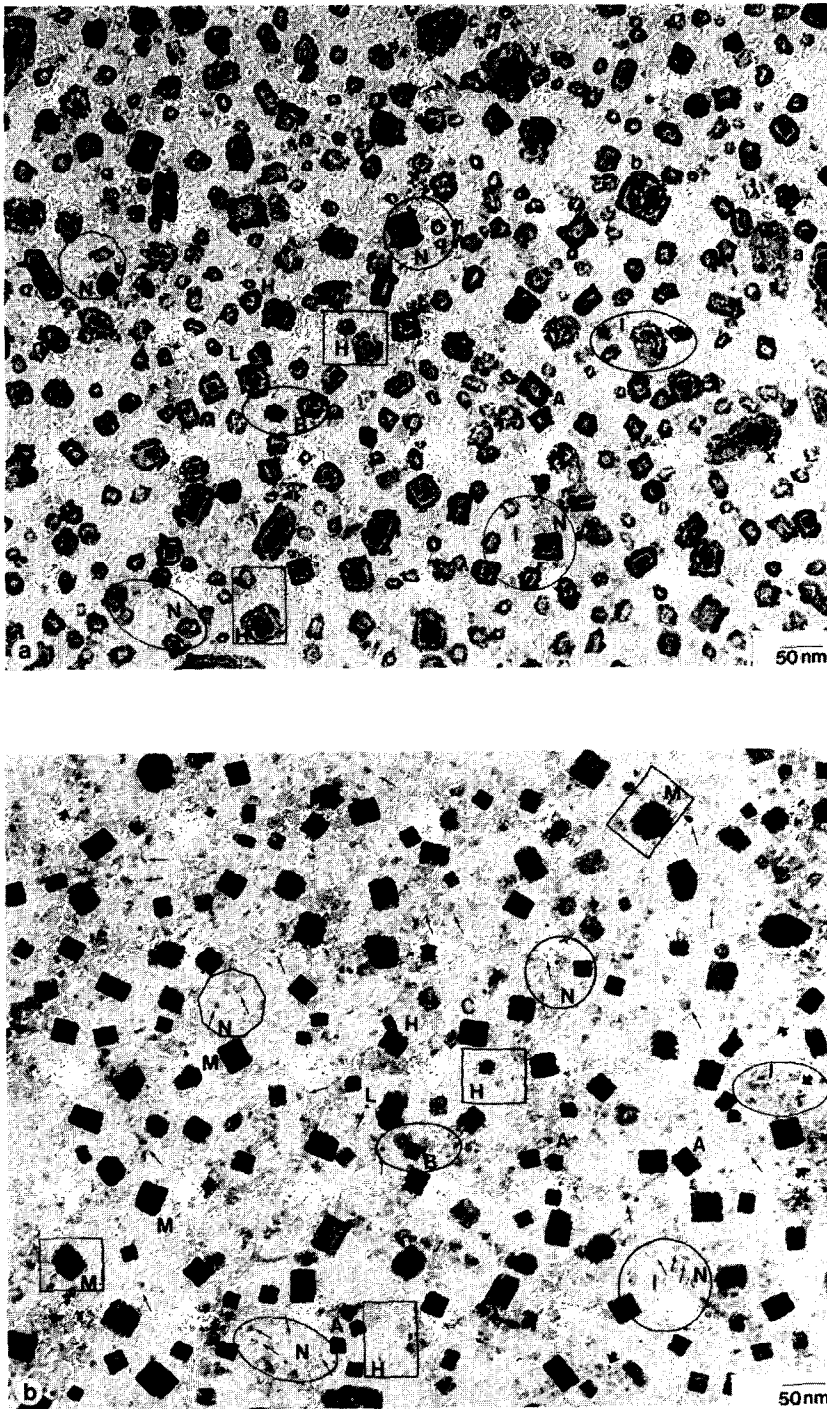
FIG. 13. Sequence of changes on heating a model Fe/Al_2O_3 specimen in purified hydrogen at progressively higher temperatures. Initial loading, 7.5 Å. The same region is shown after (a) 4 h, 400°C; (b) 2 h, 500°C; (c) 4 h, 600°C; (d) 2 h, 700°C.
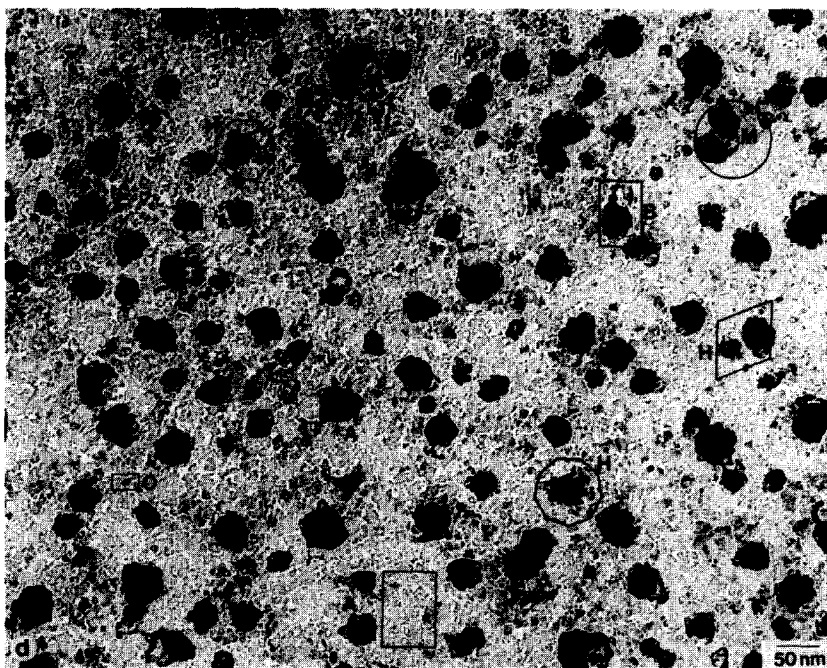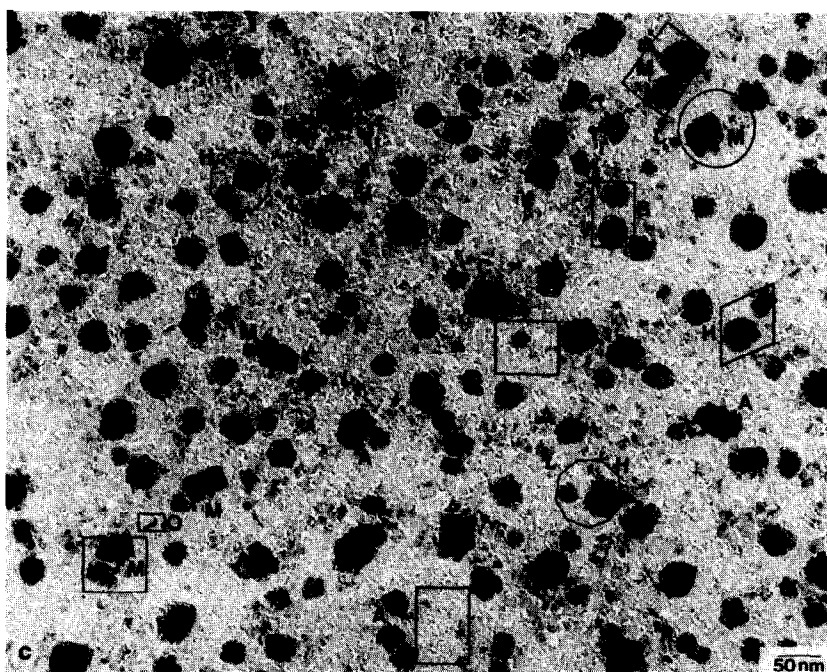
FIG. 13—*Continued.*
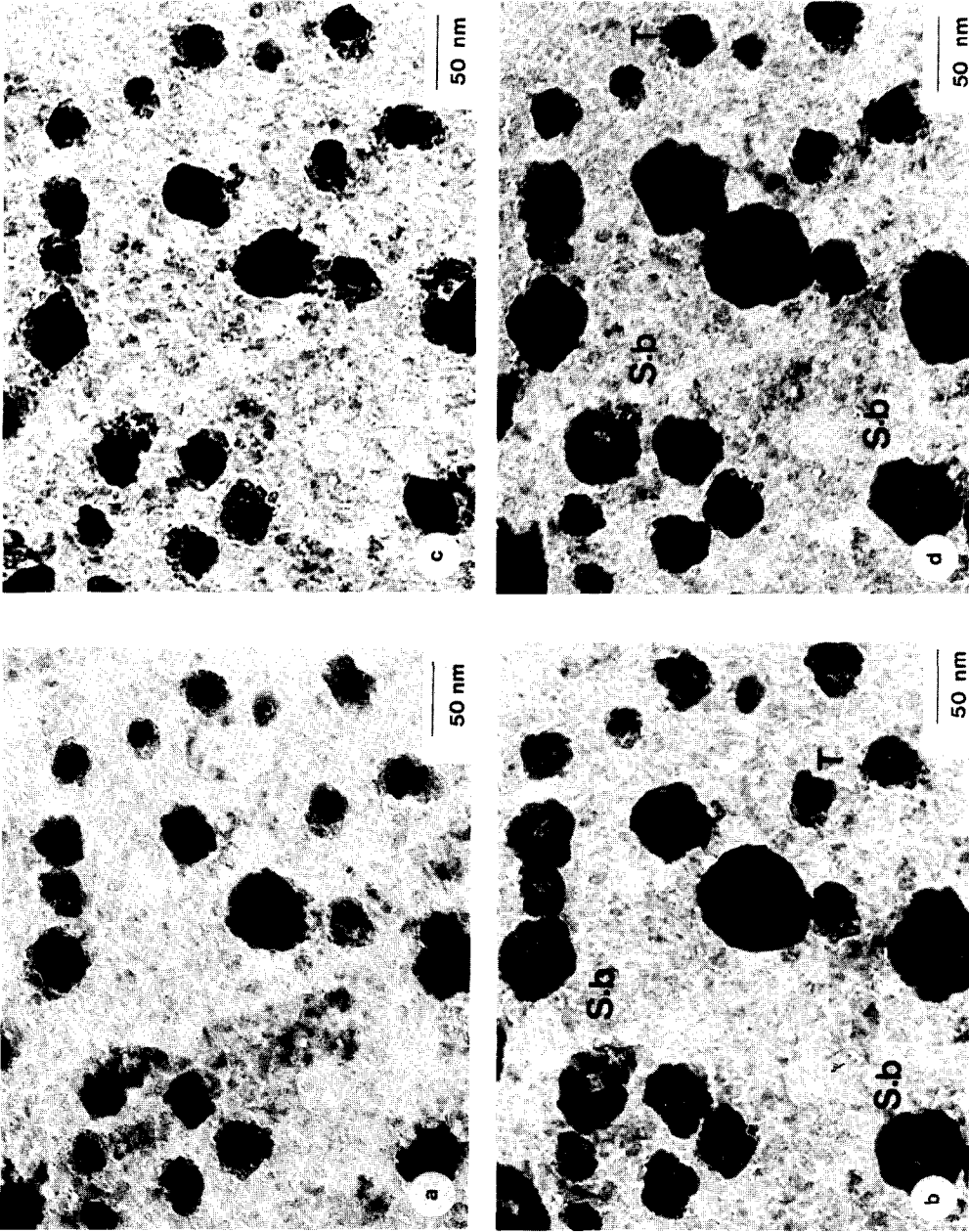
FIG. 14. Sequence of changes on heating a specimen alternately in oxygen and purified hydrogen. (a) 6 h, H_2, 600°C; (b) 1 h, O_2, 600°C; (c) 5 h, H_2, 600°C; (d) 1 h, O_2, 600°C.

TABLE 5

Alternate Heating in Oxygen and Purified Hydrogen

Heating atmosphere	Event observed	Compound identified
Table 5$_{6,500}$		
O$_2$	Particle extension. Particles have a torus shape and a film appears to fill in the cavity. (14b)	d-values approaching those of FeAl$_2$O$_4$ and Al$_2$Fe$_2$O$_6$
H$_2$	Particle contraction. Faint annular ring is observed initially and compact particles are formed on continued heating.	FeAl$_2$O$_4$ decreases in amount, α-Fe and traces of Fe$_3$O$_4$ (γ-Fe$_2$O$_3$)
Table 5$_{6,600}$		
O$_2$	Crystallites extend and assume a torus shape, enclosing a large cavity and having a small residual particle in the cavity. (14d)	Fe$_3$O$_4$ (γ-Fe$_2$O$_3$), FeAl$_2$O$_4$
H$_2$	Contraction and compact particle formation. Core-and-ring structure is not observed. (14a, c)	
Table 5$_{7.5,500}$		
O$_2$	(Heated before in hydrogen at 700°C, Fig. 13d). Considerable extension. Large cavity formation in the crystallite (S.b.). A small residual particle is present in the cavity of each crystallite. No change on prolonged heating. (15a)	FeAl$_2$O$_4$, Fe$_3$O$_4$ (γ-Fe$_2$O$_3$)
H$_2$	Splitting of some crystallites into a few interlinked particles, some having a core-and-ring structure (V). Sintering of the sub-units on further heating. (15b)	FeAl$_2$O$_4$, α-Fe, traces Fe$_3$O$_4$ (γ-Fe$_2$O$_3$)
Table 5$_{7.5,700}$		
H$_2$	Contraction and formation of more compact particles. Marks of particle peripheries (P). (15c)	FeAl$_2$O$_4$, Fe$_3$O$_4$ (γ-Fe$_2$O$_3$)
O$_2$	Considerable extension. No cavities in particles. A small residual particle is present on the extended parent crystallite (T). The substrate appears covered by a film (R). (15d)	FeAl$_2$O$_4$, Al$_2$Fe$_2$O$_6$
H$_2$	Contraction and formation of compact particles. No core-and-ring structure. (15e)	FeAl$_2$O$_4$

present before (L, N). The crystallites might have fragmented into smaller particles (including single atoms) which subsequently migrated on the substrate before colliding and coalescing with other particles. Of course, the migrating crystallites might have simultaneously lost some atoms too, thus decreasing further in size.

B.2. Alternate heating in oxygen and hydrogen. The extension following oxidation is more pronounced when purified hydrogen is used in the reduction step instead

of the as-supplied hydrogen (Sect. A.2). In addition, a few differences in the behavior of the two cases have been observed, as listed in Tables 3 and 5. The events observed in Table 5$_{7.5,700}$ are of particular interest. After 1 h of oxidation at 500°C, each crystallite extended considerably acquiring a torus shape (Fig. 15a). However, a small residual particle remained randomly located within the cavity. The leading edge of the torus has an undulating form and the torus appears to be composed of interlinked
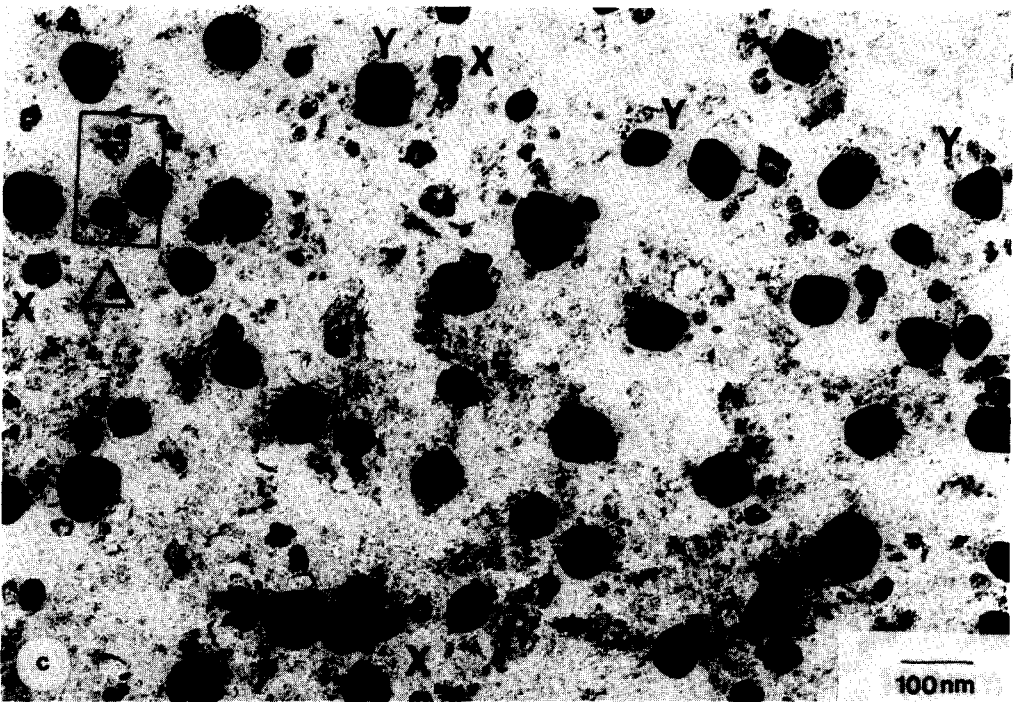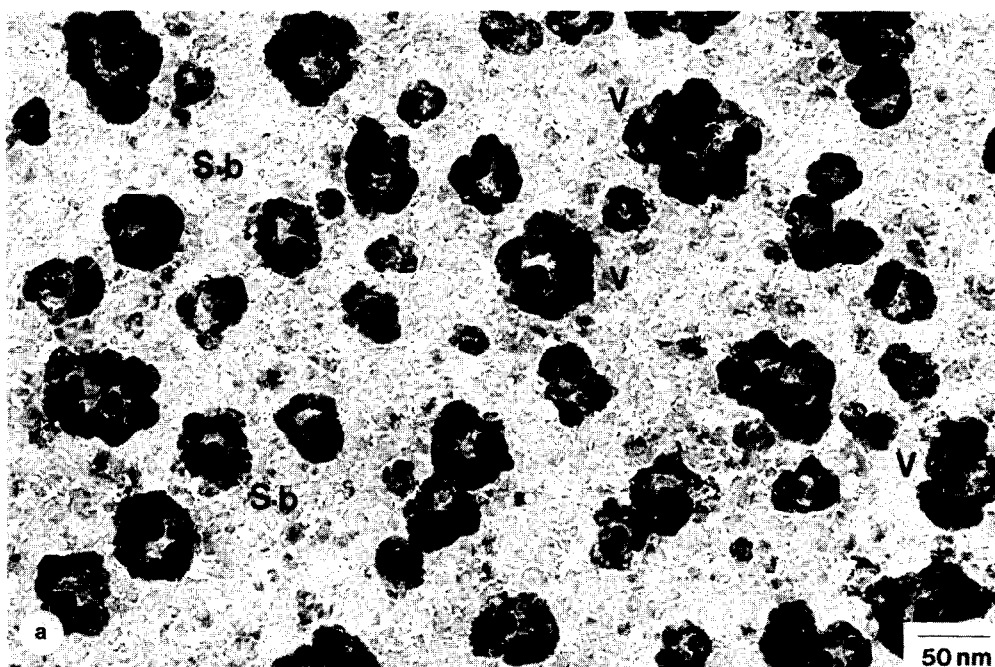
FIG. 15. Sequence of changes on heating the specimen of Fig. 13d alternately in oxygen and hydrogen. (a) 1 h, O_2, 500°C; (b) 30 min, H_2, 500°C (reduction for a longer duration followed by oxidation at the same temperature was carried out between (b) and (c)); 2 h, H_2, 700°C; (d) 12 h, O_2, 700°C (there is very little difference between 1 and 12 h oxidation); (e) 1 h, H_2, 700°C.

subunits. Heating this specimen subsequently in hydrogen at 500°C for only $\frac{1}{2}$ h caused splitting, especially of the larger crystallites, into a few interconnected subunits, some of which have a core-and-ring structure (Fig. 15b). Subsequently, the subunits sintered to form compact particles (Fig. 15c). Heating in oxygen at 700°C caused pronounced wetting and extension of the crystallites. However, unlike the previous cases, cavities were not formed (Fig. 15d). Instead, each crystallite extended as a uniformly thick film with a residual particle on top. The substrate grain boundaries also appear less distinct, probably because of a film covering the substrate, as observed also in Section A.2 on oxidation at 700°C. Subsequent heating in hydrogen at 700°C caused each particle to contract to form a single compact particle, instead of splitting into a few as observed at 500°C.

C. Effect of Moisture and Residual Oxygen Present in the as-Supplied Hydrogen

The effect of moisture on the crystallites and their composition was investigated by first purifying the as-supplied hydrogen and then bubbling it through distilled water. The effect of moisture appears to be similar to that of pure flowing oxygen. At 500°C, the crystallites extended and formed torus-shape particles. Solid solutions leading to $FeAl_2O_4$ were detected in the diffraction pattern. The effect of residual oxygen in the absence of moisture was examined by passing the as-supplied hydrogen through a desiccant. In contrast to the residual oxygen, which causes shape changes and some extension, the moisture causes much greater extension and easier aluminate formation. In other words, moisture considerably en-

FIG. 15—*Continued.*

50 nm

50 nm
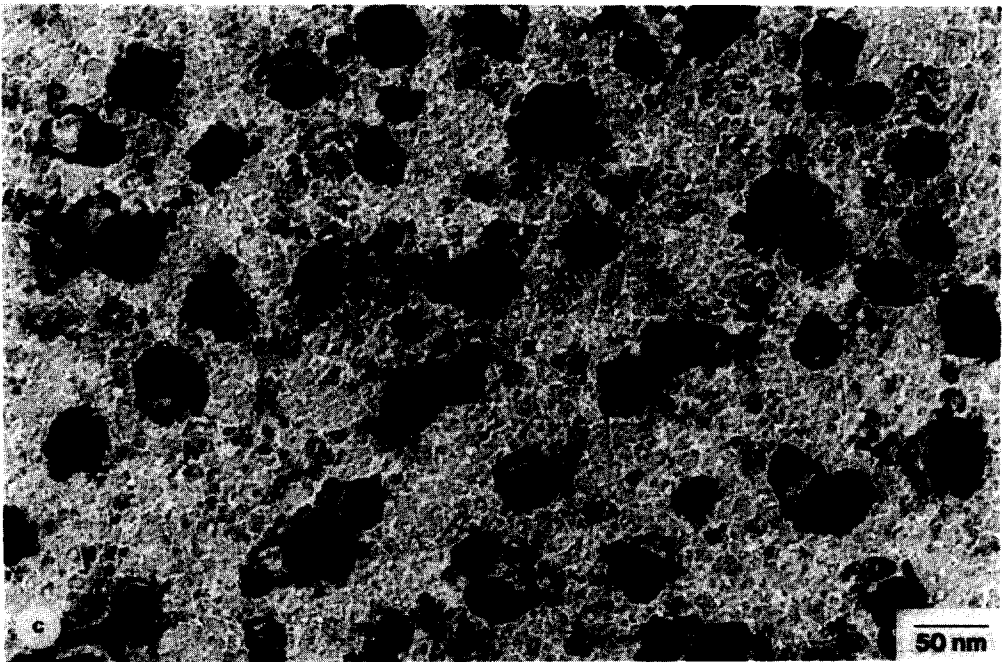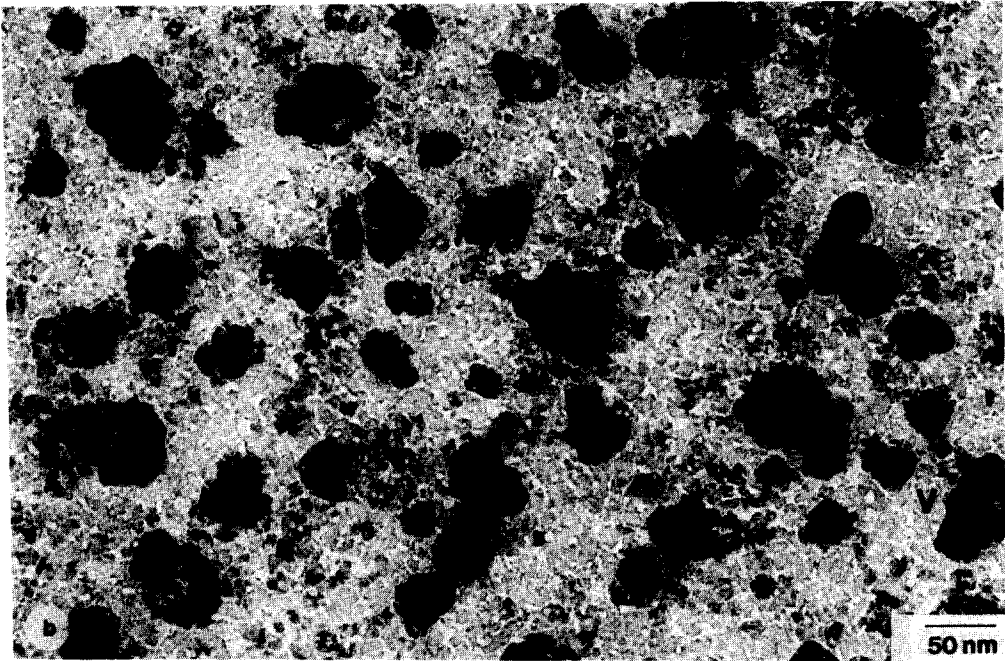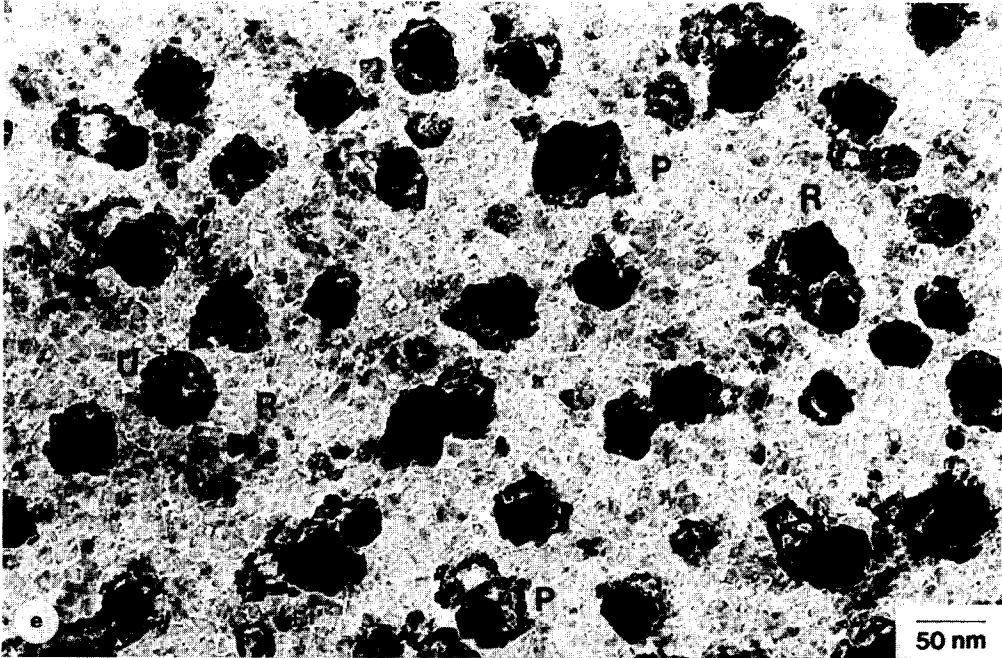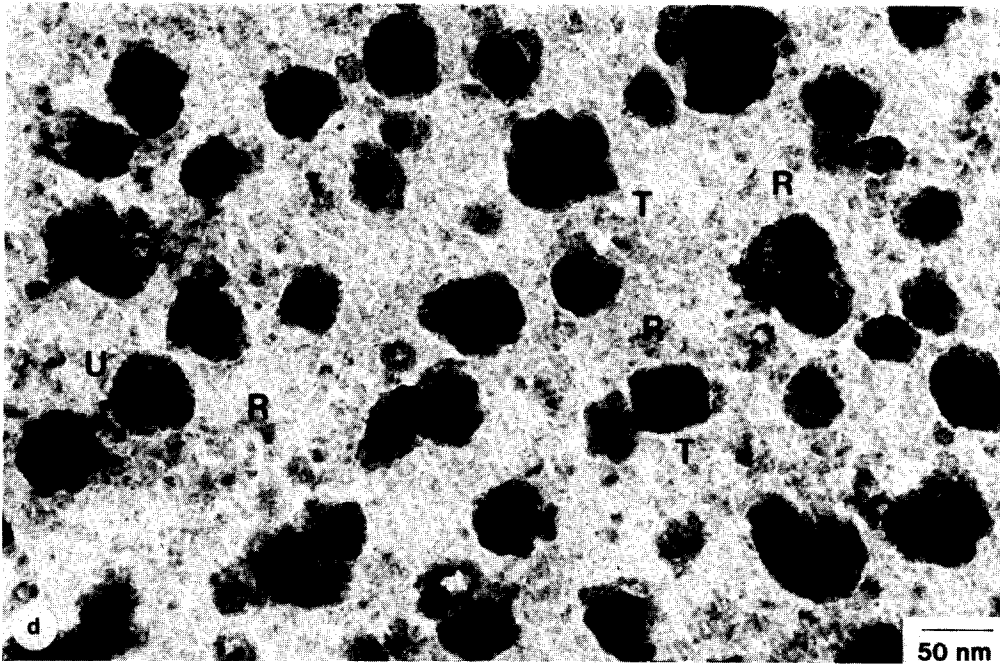
FIG. 15—*Continued*.

hances the effects caused by the residual oxygen.

DISCUSSION

The results presented in the previous section bring evidence for a variety of phenomena such as sintering, wetting and extension, shape changes, splitting, etc., which occur during heating of iron-on-alumina model catalysts. In what follows, some of these phenomena are discussed in more detail.

Sintering Behavior

The process of sintering can occur by several mechanisms (17), such as migration of crystallites and their coalescence (23), emission of single atoms by the small crystallites and their capture by the large ones (24–27), and a combination of the two (27). Two possibilities have been suggested for sintering by single-atom emission and capture. In one of them, a large number of crystallites are involved and the small crystallites lose atoms to a surface phase of single atoms dispersed over the substrate, while the large ones capture atoms from this phase. This process, known as Ostwald ripening, occurs when the substrate surface phase of single atoms is supersaturated with respect to the large crystallites and undersaturated with respect to the small ones.

In the other case, called direct ripening (28), atoms released by a small particle move directly to a neighboring large crystallite, even though the surface phase of single atoms is, on the average, undersaturated with respect to all the crystallites present. In contrast to Ostwald ripening, which is global, the latter is local and can be considered as a fluctuation from the average behavior, determined by the local surface pressures generated by the particles involved.

As seen from Table 1, migration and coalescence of crystallites (Figs. 3a–c, 7b, c, 13a–d), disappearance of a large number of small particles (Ostwald ripening, Figs. 4a–d, 12a–c) and decrease and disappearance

of a few particles near larger particles (direct ripening, Figs. 3a, b, 4'a–c) could all be detected in the present experiments. Interestingly, large crystallites appear to have migrated over large distances. For example, crystallites greater than 90 Å in size have migrated at 700°C (Figs. 6a–d). Also, crystallites of about 480 Å migrated over distances of about 600 Å at 800°C (Figs. 7b, c). Even though the number of particles whose migration could be detected is small, the few instances of migration of large particles over large distances, the redistribution of particles sometimes observed (Figs. 6d–f, 7b, c), the appearance of dumbbell-shape particles (Fig. 3c), and the appearance of small particles in regions unoccupied before (Figs. 6e, f; 12a–d; 13a–c) indicate that migration, more likely of the smaller crystallites, plays a role in the sintering phenomenon. Similarly, a large number of small as well as large crystallites disappear at temperatures as low as 400 or 500°C. In addition to the ripening mechanism, the disappearance of these small particles may be caused by their considerable extension to an undetectably thin film which subsequently coalesces with the nearby particles, or by their migration following fragmentation. In fact, in some cases, a surface film (instead of a surface phase of single atoms) appears to coexist with the three-dimensional crystallites. As pointed out in a previous section (Sect. B.1), the disappearance of the small particles from some regions and the appearance of other, new particles in regions far removed from the previous indicate that mechanisms other than just migration and coalescence (which is expected to occur over only shorter distances), or ripening (since contrary to what is predicted by ripening, large particles have vanished while smaller ones remained (H in Figs. 3b, c, 15a, b)) probably occur. Other mechanisms, such as fragmentation followed by migration of the smaller fragments (N in Figs. 6d–f), emission of atoms from the migrating crystallites, considerable extension

to an undetectable film which splits and contracts to form new particles, etc., might have also occurred. The last process occurs, either because of alternate oxidation and reduction in the as-supplied hydrogen, and/or because of the heterogeneities of the substrate which interacts strongly with the particles in some regions and weakly in other regions.

Wetting Behavior

It is important to recognize that the wetting characteristics of the crystallites on the support affect the sintering and redispersion behavior, the thermostability of the size distribution, and the shape of the crystallites. The role of wetting in the redispersion of supported metal crystallites and in the changes of their shape has been emphasized in Refs. (*19, 20, 23, 29*).

Wetting angle. The ability of a crystallite to wet a support and its extent are determined by the equilibrium of the three interfacial tensions, substrate–gas (σ_{sg}), crystallite–gas (σ_{cg}), and crystallite–substrate (σ_{cs}), as expressed by Young's equation

$$\sigma_{sg} - \sigma_{cs} = \sigma_{cg} \cos \theta, \qquad (1)$$

where θ is the equilibrium wetting or contact angle. When, under some conditions such as oxidizing,

$$\sigma_{sg} - \sigma_{cs} > \sigma_{cg} \qquad (1a)$$

is satisfied, no wetting angle can exist, since $\cos \theta > 1$, and the crystallite spreads over the substrate. On the other hand, when

$$\sigma_{sg} - \sigma_{cs} < \sigma_{cg} \qquad (1b)$$

is satisfied, the crystallite forms an equilibrium contact angle, θ, with the substrate, whose value lies in the range $0° < \theta < 180°$, depending upon both the difference ($\sigma_{sg} - \sigma_{cs}$) as well as σ_{cg}. Under vacuum, in inert, or reducing atmospheres, the metals which are commonly used as supported catalysts have, in general, a high surface tension σ_{cg}, as well as a high interfacial tension, σ_{cs}, with silica and alumina supports (*30, 31*). These lead to contact angles

greater than 90° and the crystallites do not wet well the support. However, in an oxidizing environment both σ_{cg} and σ_{cs} are smaller, since these values are smaller for the oxide compared to those of the corresponding metal, and the contact angle can decrease. Accordingly, the crystallite will extend and wet the support better.

Interaction energy and wetting. When two phases are brought into contact to form an interface, and there are no molecular interactions between them, the interfacial tension between the two should be expressed by the sum

$$\sigma_{cs} = \sigma_c + \sigma_s. \qquad (2)$$

However, there are always attractive molecular interactions between two phases brought into contact and because of this, there is a corresponding decrease in the interfacial tension. These interactions are strong when they are of a chemical nature, for instance, the formation of compounds, or weak when they are of a physical nature, such as dispersion or polar interactions. The interfacial tension between crystallite and substrate is therefore given by

$$\sigma_{cs} = \sigma_c + \sigma_s - (U_{int} - U_{str})$$
$$= \sigma_c + \sigma_s - U_{cs}, \qquad (3)$$

where, U_{int} is the interaction energy per unit area of crystallite–substrate interface between the atoms or molecules of the crystallite and those of the substrate and U_{str} is the strain energy per unit area arising as a result of the mismatch of the two lattices.

When a chemical interaction takes place at the crystallite–substrate interface (leading to the formation of a compound), as in the case of iron on alumina in an oxidizing environment, U_{cs} will become large, thereby appreciably decreasing σ_{cs}. In fact, if the chemical bonding at the interface is very strong, U_{cs} will become so large that σ_{cs} can decrease to zero or (under nonequilibrium conditions) even below zero. Such a large decrease in the dynamic interfacial tension, σ_{cs}, and also a concomitant decrease in the value of σ_c (in an oxidizing

environment the metal forms an oxide, and σ_c of the oxide is smaller than σ_c of the metal) lead to a rapid spreading of the crystallite over the substrate, since the driving force for spreading ($\sigma_{sg} - \sigma_{cs} - \sigma_{cg} \cos \theta$) is considerably increased.[3] Initially, the reaction occurs only at the interface and then it proceeds in the bulk of either the substrate or the crystallite, more likely the former. Bulk reaction occurs because it decreases the free energy of the system and it continues until the rate of dissolution of the oxide molecules into the substrate is considerably limited by the diffusional resistance. Immediately following the reaction at the interface, the crystallite is probably present in a highly extended and unstable configuration because of the large driving force for spreading. Any thinning produced by perturbations (such as diffusion into the substrate, thermal fluctuations, etc.) will tend to grow, leading finally to the torus which, under the conditions of the experiment, might be the thermodynamically stable configuration. The rapid extension following the initial surface reaction is soon arrested since, subsequently, U_{cs} is relatively reduced. Indeed, after some of the oxide has already dissolved into the substrate, the subsequent surface interaction energy, U_{cs}, between the aluminate and the oxide is no longer as large as that between alumina and oxide, since, unlike the latter, the former does not lead to a chemical compound at the interface. Consequently, the driving force for spreading $\{\sigma_{sg} - (\sigma_s + \sigma_c - U_{cs}) - \sigma_{cg} \cos \theta\}$ becomes smaller. To summarize, σ_{cs} has a large decrease initially, even possibly becoming negative, and then increases. Correspondingly, the initial large driving force for spreading also decreases subsequently. Therefore, the considerably extended crystallite formed by the initial rapid extension subsequently reaches a new equilibrium wetting angle with the new layer of substrate (reaction product) at the (crystallite–substrate) inter-

---

[3] Here θ is the instantaneous nonequilibrium wetting angle.
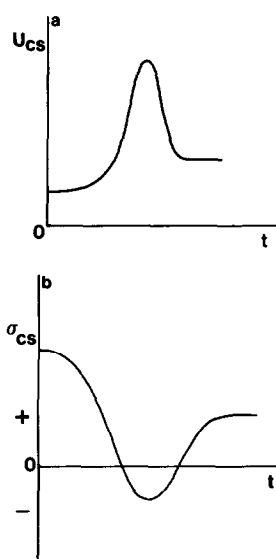
FIG. 16. Schematic of the variation with time of (a) the interaction energy, U_{cs}, and (b) the crystallite–substrate interfacial tension, σ_{cs}, when there is a chemical reaction between the crystallite and the substrate.

face. The time evolution of U_{cs} and σ_{cs} are shown schematically in Fig. 16.

If a small cavity had initially nucleated in the extended crystallite because of the rapid extension and the dissolution of a part into the substrate, the subsequent tendency to form a larger wetting angle, for reasons just described above, would make both the inner and the outer leading edges of the cavity-containing crystallite to withdraw. This causes the expansion of the cavity and leads to the observed torus shape. It should be noted, however, that depending upon the substrate material (aluminate or alumina) ahead of each of the two leading edges being the same or different, the final equilibrium angles at the outer and inner edges of the torus may be the same or different. In addition, as a result of the rapid extension, the crystallite may undergo fragmentation and the torus may appear to be composed of interconnected smaller units (Figs. 9d, 9f). On the other hand, if the interactions at the leading edge with the substrate are very strong so as to bind the crystallite to the substrate and if for some reasons the initial cavity does not form in

the extended crystallite, then the subsequent tendency to contract following reduction would generate opposing forces, since the crystallite tends to contract while its periphery is constrained from following through. This generates the annular gap and gives rise to the core-and-ring structure (*32*). This tendency is enhanced by temperatures which are sufficiently low so as not to break the binding at the crystallite periphery. If the temperature is high, however, the binding at the periphery can be broken and the particle will contract as a single unit to form a compact structure. Compact particles and marks of their previous particle peripheries on the substrate were indeed observed at the high temperatures of 700 and 800°C (Figs. 6d; 7c; 11a, b) (and also at 500°C but at higher loading or when pure hydrogen was used for reduction, Figs. 9c, 15c). From the above discussion it results that depending upon the kinetics of the different processes (such as dissolution, reaction, wetting etc.) either a torus shape or a core-and-ring structure may form initially. Subsequent alternation between these shapes, observed with Fe/Al_2O_3 heated in as-supplied hydrogen, is a result of alternate oxidation and relative reduction and is discussed in Refs. (*22, 32*). The events observed in the present experiments can be explained on the basis of the above strong chemical interaction and wetting considerations as follows.

Iron does not wet alumina in reducing or inert atmospheres when there is no reaction or mass transfer at the interface, its wetting angle near the melting point being 141° (*31, 33*). However, in either partially or fully oxidizing environments, such as hydrogen contaminated with oxygen and/or moisture (even only in traces) or flowing oxygen, the present results indicate that the crystallites are extended. Electron diffraction indicates that in both the oxidizing environments, in addition to some oxide (γ-Fe_2O_3 (Fe_3O_4)), an interaction product, probably a solid solution of iron oxide in alumina and/or vice versa, is formed. The

reactivity of iron, in general, with oxygen is very high. In the case of supported iron (iron supported on alumina), oxygen, even present only in traces, is preferentially adsorbed at the interface (*34*), decreasing both σ_{cg} and σ_{cs}. This decreases θ and the crystallite extends on the alumina surface. An additional decrease in σ_{cs} occurs as a result of the interaction of the iron ions with the alumina support. Alumina, especially the γ form, possesses a defect structure and a dehydroxylated surface (*35*) and is therefore very reactive. At low loadings, the iron ions move into the vacant sites of γ-Al_2O_3. The solubility of Fe^{3+} ions in γ-Al_2O_3 can be appreciable because of the chemical similarity of the cations and also the availability of defects in γ-Al_2O_3. As a result of this metal oxide reaction with alumina, a strong chemical bonding results between the crystallite and the support, and U_{cs} is tremendously increased. Such strong interactions lead to the observed extended forms and the torus or core-and-ring shapes as described in the previous paragraphs. However, although they prevent subsequent sintering, such strong interactions with the support cause difficulties in reducing the iron ions to the zero-valent metal. The reaction products, either the solid solutions of iron oxide with alumina or the stoichiometric aluminates, $FeAl_2O_4$ and $Al_2Fe_2O_6$, are very difficult to be reduced (as seen in Tables 2–5) compared to the pure oxide of iron. In fact, iron oxide itself requires only 300°C for reduction to the metallic state (*12*). The literature (*6, 16*) also indicates that ferric ions supported on Al_2O_3 or silica in low concentrations (about 0.1 wt%) can be only partially reduced by hydrogen to the ferrous state, even at 700°C. Direct evidence for the formation, at low loadings, of the difficult-to-reduce aluminates or solid solutions in the presence of even traces of oxygen and/or moisture has been indicated by electron diffraction in the present experiments (Tables 2–4). Their presence could explain the difficulty encountered in the literature to reduce Fe^{3+} ions below the Fe^{2+} state at tem-

peratures as high as 700°C, if the reducing hydrogen contained even traces of oxygen or moisture. Other factors in the catalyst preparation procedure, such as the precursor used, pH, etc., may facilitate the formation of such compounds. On the other hand, if the loading is large, initially large particles form, which have a relatively smaller fraction of their atoms in contact with the substrate at the interface. The interaction compounds (aluminates or solid solutions) formed between the two will be in relatively small amounts compared to the oxide. Therefore they are not easily detected by electron diffraction and they do not pose difficulties in reducing the oxide to the metal, even at the relatively low temperature of 500°C. Hence, in such cases the oxide particles are reduced easily (α-Fe is detected by electron diffraction) and the reduced crystallites will have relatively weak interactions with the substrate. As a result, considerable sintering occurs and dense, compact particles are formed (Fig. 4d). In fact, when further purified hydrogen is used during the reduction step, formation of compact particles and reduction to α-Fe occur even for relatively low loadings even at the low temperatures of 500°C (Table 13). This occurs because of decreased interaction between crystallite and support in the absence of oxygen and/or moisture.

A thick film extends from around the particles on heating in oxygen at 700°C and only aluminate is detected in the diffraction pattern. A thick film of aluminate may cover the alumina substrate if $\sigma_{\text{aluminate–gas}}$ + $\sigma_{\text{aluminate–alumina}}$ < $\sigma_{\text{alumina–gas}}$. Similarly, a thick film of aluminate may cover the oxide particles if $\sigma_{\text{aluminate–gas}}$ + $\sigma_{\text{aluminate–iron oxide}}$ < $\sigma_{\text{iron oxide–gas}}$.

As seen in Figs. 14 and 15 the degree of extension of the crystallites, when they are heated in flowing oxygen, is higher at 700°C than at 600 and 500°C. The fact that the temperature coefficients of surface and interfacial tensions are negative for most materials (σ_{cg}, σ_{cs}, and σ_{sg} decrease with increasing temperatures) and the possibility

of an enhanced reaction between the gas, the crystallite, and the substrate at higher temperatures may explain this observation. (Of course, this implies sufficient decreases with temperature of σ_{cs} and/or σ_{cg} compared to that of σ_{sg}.) In fact, it is possible that heating the crystallites in oxygen at temperatures higher than 700°C will cause even more extension, and eventually complete spreading. This can happen if the inequality (1a) is satisfied but will be observed only if the time needed for complete spreading is shorter than the heating time.

SMSI

The SMSI (strong metal–support interactions) referred to frequently in the recent literature (36) is in reality (as already noted by Ruckenstein and Pulvermacher (23)) a reflection of the quantity U_{cs}, which in turn is related via Eq. (3) to the interfacial tension σ_{cs}. Large values of U_{cs}, hence strong interactions (23) lead to small values of σ_{cs} (even to negative values of σ_{cs} under nonequilibrium conditions). As a result, a variety of surface phenomena associated with wetting and spreading, of the kind discussed in Ref. (23) and in this paper, occur.

Splitting Behavior

Splitting of crystallites has been observed under different conditions and in different forms (Tables 1–3, 5). When heated in as-supplied hydrogen at 400°C, some crystallites were observed to split into two and to merge again subsequently (M in Figs. 2g–i). The crystallites had a torus shape both before as well as after the splitting. Such splitting may be a result of the extension and the instability of the extended toroidal shape to local variations in curvature along the periphery. Following heating in oxygen, in the majority of cases, the crystallites appear to be composed of a number of smaller subunits held together (Figs. 9d, 9f). Such a breakup is more likely a result of the spreading generated stresses and rupture (20, 28). Palladium crystallites on alumina

were also observed to become porous and develop cavities when heated in oxygen (*18–20*). It was shown that if the crystallites were small or if the temperature was high, the crystallites extended irregularly, exhibiting a kind of tearing phenomenon.

The extension of the crystallites following oxidation generates stresses in the crystallite and leads to the growth of existing cracks if these stresses exceed the critical stress for crack propagation given by Griffith's expression

$$\tau_c = \left(\frac{2E\gamma}{\pi r}\right)^{1/2},$$

where γ is the surface tension, r is a characteristic length of the crack, and E is Young's modulus of elasticity. Further oxidation, especially at the tip of the cracks, facilitates the crack propagation and the crystallite is ruptured and appears to be made up of disjointed smaller units. However, because iron oxide has a tendency to wet alumina, the individual units of the crystallites may be very near to one another. Splitting is, therefore, not observed clearly in oxidizing atmospheres, but the crystallites appear porous. Subsequent heating in hydrogen tends to contract the particle and the splitting becomes evident as each individual unit tends to contract to a higher equilibrium wetting angle. Of course, on continued heating in hydrogen the individual crystallites coalesce and sinter together.

Redisperion of the crystallites may also occur as a result of rupture and contraction of an extended surface film. As seen in Figs. 12c and 15d a kind of thick film either of iron oxide or of aluminate may spread on alumina from the periphery of the crystallites. In an oxygen atmosphere there may even be a multilayer surface film on the surface of alumina, coexisting with the three-dimensional crystallites. The film may not be continuous, but ruptured. When heated subsequently in hydrogen, the islands will contract to a higher equilibrium angle. During this process of contraction a part of the film may coalesce with the adjacent parti-

cles and a part may form new, smaller crystallites, effectively causing redispersion.

The fragmentation of the crystallites to a large number of smaller particles observed after repeated alternate heating in hydrogen and oxygen for a total of about 200 h (Figs. 9f and g) is again a result of the spreading generated stresses and rupture. If a chemical interaction occurs between the crystallites and the substrate, repeated alternations may modify the support and affect the wetting behavior of the crystallites as a result of the repeated diffusion of the iron oxide molecules in and out of the substrate. In addition, the fragmentation may be influenced by the mechanical fatigue that sets in the crystallites due to repeated extensions and contractions.

CONCLUSION

Several phenomena have been observed to occur during heating model iron/alumina catalysts in hydrogen containing trace amounts of oxygen and/or moisture, in additionally purified hydrogen, and in oxygen. Particle growth by migration and coalescence, by emission and capture of atoms involving only a few neighboring crystallites (direct ripening) as well as a large number of the crystallites (Ostwald ripening) have been observed. These are, however, only a part of the complex surface phenomena that occur. Coalescence of nearby particles, extension and disappearance of particles, appearance of new particles in regions unoccupied previously, and splitting of particles also occur. In addition, ppm quantities of oxygen and/or moisture in hydrogen are shown to affect the reducibility of the iron ions and also to cause stability with respect to growth of the crystallites. Electron diffraction indicated considerable chemical interaction of the crystallites with the support and indicated the formation of solid solutions of iron oxide with alumina or of the stoichiometric aluminates $FeO \cdot Al_2O_3$ and $Fe_2O_3 \cdot Al_2O_3$. As a result of these chemical interactions, the crystallites have been observed to undergo

changes in shape alternately from a torus to a core-and-ring structure when heated, especially at low temperatures of 400 or 500°C, in ultrahigh pure hydrogen containing trace quantities of oxygen and/or moisture. Such alternations were not observed when hydrogen was further purified to minimize oxygen and moisture contents. The additionally purified hydrogen caused better reducibility to the zero-valent metal. On heating in as-supplied hydrogen, at the low loadings of 6 or 7.5 Å, very little Fe^0 forms even at 700°C, whereas almost complete reduction to metallic iron is achieved even at 500°C when the loading is high, about 12.5 Å. In contrast, with additionally purified hydrogen, metallic iron could be detected even at 400°C for a loading of only 7.5 Å. On heating in oxygen, the crystallites were observed to extend considerably, the extension being enhanced with increasing temperatures. Toroidal shapes with a small remnant particle in the cavity were observed on heating in oxygen at 500 and 600°C. The extent of wetting increased at 700°C. In addition, it was inferred from the electron micrographs that on heating in oxygen at 700°C, a film whose thickness should be greater than monomolecular, coexists with three-dimensional crystallites. After prolonged alternate heating in hydrogen and oxygen, the crystallites were observed to split into a number of smaller particles, probably as a result of mechanical fatigue. The results are discussed in terms of the interactions between metal, gas, and support and the consequent wetting characteristics of the metal–support system. It is suggested that such strong chemical interactions may lead to a considerable decrease in the interfacial tension between crystallite and substrate and, therefore, to a tendency for the crystallites to spread out. It is stressed that the strong metal–support interaction, the sintering and redispersion phenomena, and the changes in the shape of the crystallites are all interlinked parts of a complex surface phenomenon that cannot be easily categorized as belonging to a simple "either or" phenomenon.

REFERENCES

1. Anderson, J. R., "Structure of Metallic Catalysts." Academic Press, New York, 1975.
2. Satterfield, C. N., "Heterogeneous Catalysis in Practice." McGraw–Hill, New York, 1980.
3. Amelse, J. A. Butt, J. B., and Schwartz, L. H., *J. Phys. Chem.* **82**(5), 558 (1978).
4. Guczi, L., *Catal. Rev.-Sci. Eng.* **23**(3), 329, (1981).
5. Yoshioka, T., Koezuka, J., and Ikoma, H., *J. Catal.* **16**, 264 (1970).
6. Garten, R. L., and Ollis, D. F., *J. Catal.* **35**, 232 (1974).
7. Brenner, A., and Hucul, D. A., *Inorg. Chem.* **18**(10), 2836 (1979).
8. Raupp, G. B., and Delgass, W. N., *J. Catal.* **58**, 337 (1979).
9. Raupp, G. B., and Delgass, W. N., *J. Catal.* **58**, 348 (1979).
10. Vannice, M. A., *J. Catal.* **37**, 462 (1975).
11. Perrichon, V., Charcosset, H., Barrault, J., and Forquy, C., *Appl. Catal.* **7**, 21 (1983).
12. Topsøe, H., Dumesic, J. A., and Morup, S., in "Applications of Mössbauer Spectroscopy" (R. L. Cohen, Ed.), Vol. 2. Academic Press, New York, 1980.
13. Raupp, G. B., and Delgass, W. N., *J. Catal.* **58**, 361 (1979).
14. Amelse, J. A., Grynkevich, G., Butt, J. B., and Schwartz, L. H., *J. Phys. Chem.* **85**, 2484 (1981).
15. Hobson, M. C., Jr., and Gager, H. M., *J. Catal.* **16**, 254 (1970).
16. Garten, R. L., *J. Catal.* **43**, 18 (1976).
17. Ruckenstein, E., and Dadyburjor, D. B., *Reviews in Chem. Eng.* **1**, 251 (1983).
18. Chen, J. J., and Ruckenstein, E., *J. Catal.* **69**, 254 (1981).
19. Ruckenstein, E., and Chen, J. J., *J. Colloid Interface Sci.* **86**(1), 1 (1982).
20. Chen, J. J., and Ruckenstein, E., *J. Phys. Chem.* **85**, 1696 (1981).
21. Chu, Y. F., and Ruckenstein, E., *J. Catal.* **41**, 385 (1976).
22. Sushumna, I., and Ruckenstein, E., *J. Catal.* **90**, 241 (1984).
23. Ruckenstein, E., and Pulvermacher, B., *J. Catal.* **29**, 224 (1973).
24. Chakraverty, B. K., *J. Phys. Chem. Solids* **28**, 2401 (1967).
25. Wynblatt, P., and Gjostein, N. A., *Progr. Solid State Chem.* **9**, 21 (1975).
26. Flynn, P. C., and Wanke, S. E., *J. Catal.* **34**, 390 (1974).
27. Ruckenstein, E., and Dadyburjor, D. B., *J. Catal.* **33**, 233 (1977).
28. Ruckenstein, E., and Dadyburjor, D. B., *Thin Solid Films* **55**, 89 (1978).
29. Ruckenstein, E., and Chu, Y. F., *J. Catal.* **59**, 109 (1979).

30. Overbury, S. H., Bertrand, P. A., and Somorjai, G. A., *Chem. Rev.* **75**(5), 547 (1975).

31. Beruto, D., Barco, L., and Passerone, A., *in* "Oxides and Oxide Films" (Ashok K. Vijh, Ed.), Vol. 6. Dekker, New York, 1981.

32. Ruckenstein, E., and Sushumna, I., "Proceedings, 9th Iberoamerican Symposium on Catalysis," Vol. II, p. 1074, July (1984).

33. Naidich, Ju. V., *in* "Progress in Surface and Membrane Science" (D. A. Cadenhed and J. F. Danielli, Eds.), Vol. 14, p. 354. Academic Press, New York, 1981.

34. Halden, F. A., and Kingery, W. D., *J. Amer. Ceram. Soc.* **59**, 557 (1955).

35. Maciver, D. S., Tobin, H. H., and Barth, R. T., *J. Catal.* **2**, 485 (1963); **3**, 502 (1964).

36. Imelik, B., *et al.* (Eds.), "Studies in Surface Science and Catalysis," Vol. 11. Elsevier, Amsterdam, 1982.